DISEASES AND DISORDERS

α-Ketoglutaric acid ameliorates hyperglycemia in diabetes by inhibiting hepatic gluconeogenesis via serpina1e signaling

Yexian Yuan[1]†, Canjun Zhu[1]†, Yongliang Wang[2]†, Jia Sun[3], Jinlong Feng[1], Zewei Ma[1], Penglin Li[1], Wentong Peng[1], Cong Yin[1], Guli Xu[1], Pingwen Xu[4], Yuwei Jiang[5], Qingyan Jiang[1]*‡, Gang Shu[1]*‡

Previously, we found that α-ketoglutaric acid (AKG) stimulates muscle hypertrophy and fat loss through 2-oxoglutarate receptor 1 (OXGR1). Here, we demonstrated the beneficial effects of AKG on glucose homeostasis in a diet-induced obesity (DIO) mouse model, which are independent of OXGR1. We also showed that AKG effectively decreased blood glucose and hepatic gluconeogenesis in DIO mice. By using transcriptomic and liver-specific *serpina1e* deletion mouse model, we further demonstrated that liver *serpina1e* is required for the inhibitory effects of AKG on hepatic gluconeogenesis. Mechanistically, we supported that extracellular AKG binds with a purinergic receptor, P2RX4, to initiate the solute carrier family 25 member 11 (SLC25A11)–dependent nucleus translocation of intracellular AKG and subsequently induces demethylation of lysine 27 on histone 3 (H3K27) in the *seprina1e* promoter region to decrease hepatic gluconeogenesis. Collectively, these findings reveal an unexpected mechanism for control of hepatic gluconeogenesis using circulating AKG as a signal molecule.

INTRODUCTION

Type 2 diabetes mellitus (T2DM) is a growing global health problem, which decreases life spans through premature morbidity or mortality from associated metabolic diseases (*1*). Previous studies have shown that exercise improves glucose homeostasis partially through exercise-induced myobolites (or muscle-derived metabolites). These muscle-derived metabolites are potential therapeutic targets for T2DM, which actively prevents glycemic-related diseases by acting as exercise mimetics. While metabolite therapies for T2DM are emerging, metabolite-induced beneficial effects on glucose homeostasis still face a major obstacle of low long-term therapeutic efficiency. Here, we aim to identify the essential muscle-derived metabolites mimicking the long-term potent antidiabetic effects of regular physical exercise.

α-Ketoglutaric acid (AKG) is a citric acid cycle intermediate also known as 2-oxoglutarate. It has been shown to play a vital role in a variety of biological processes, including intestinal innate immunity (*2*), antioxidative defense (*3*), energy production (*4*), epigenetic modification (*5*), and tumor suppression (*6*). We recently found that 2% AKG water supplementation effectively prevents diet-induced obesity (DIO) by increasing brown adipose tissue temperature, oxygen consumption, and whole-body metabolism in a 2-oxoglutarate receptor 1 (OXGR1)–dependent mechanism (*7*). Notably, data from high-fat diet (HFD)–fed middle-aged mice (*8*) and DIO rats (*9*) highlight that this keto-acid also contributes to glucose tolerance and insulin sensitivity. These studies consistently demonstrated beneficial effects of AKG on metabolic balance and glucose homeostasis. However, the molecular mechanism underlying the effects of AKG on glycemic control remains unclear.

In this study, we found that serum AKG is negatively correlated with human plasma glycated hemoglobin A1c (HbA1c), the standard diabetic management biomarker for diabetic patients (*10*). Consistently, in DIO, chemical-induced type 1 diabetes (T1D), and *db/db* (DB) mouse models, AKG supplementation significantly decreased the activity of liver gluconeogenesis enzyme flux and ameliorated hyperglycemia. Using in vitro hepatocyte and liver slice culture models, we showed that AKG directly suppresses hepatic gluconeogenesis by inhibiting rate-limiting enzymes. We subsequently identified *serpina1e* (serine or cysteine peptidase inhibitor, clade A, member 1e) as a transcriptomic signature induced by AKG treatment in the liver. We further indicated that AKG promotes serpina1e expression by decreasing the trimethylation of lysine 27 on histone 3 (H3K27me3) in the seprina1e promoter region. By using a liver-specific seprina1e deletion mouse model, we established the key role of serpina1e in AKG-induced suppression on hepatic gluconeogenesis and hyperglycemia in DIO mice. Last, we found that purinergic receptor P2RX4 and intracellular AKG transporter SLC25A11 are required for the regulatory effects of extracellular AKG on gluconeogenesis in primary hepatocytes. Overall, our studies established a vital role of AKG in glucose homeostasis and identified the AKG-serpina1e pathway as potential therapeutic targets to mitigate T2DM.

RESULTS

AKG is negatively correlated with blood glucose

Previous studies showed that AKG is increased by resistance exercise and negatively correlated with human body mass index (*7*). Here, we found that plasma AKG concentrations in male mice

[1]Guangdong Laboratory of Lingnan Modern Agriculture and Guangdong Province Key Laboratory of Animal Nutritional Regulation, National Engineering Research Center for Breeding Swine Industry, College of Animal Science, South China Agricultural University, 483 Wushan Road, Tianhe District, Guangzhou, Guangdong 510642, China. [2]Key Laboratory of Animal Genetics, Breeding and Reproduction of Shaanxi Province, College of Animal Science and Technology, Northwest A&F University, Yangling, Shaanxi, China. [3]Department of Endocrinology, Zhujiang Hospital, Southern Medical University, Guangzhou 510280, China. [4]Division of Endocrinology, Department of Medicine, The University of Illinois at Chicago, Chicago, IL 60612, USA. [5]Department of Physiology and Biophysics, The University of Illinois at Chicago, Chicago, IL 60612, USA.
*Corresponding author. Email: shugang@scau.edu.cn (G.S.); qyjiang@scau.edu.cn (Q.J.)
†These authors contributed equally to this work as co-first authors.
‡Lead contact.

(a population including chow-fed C57BL/6 mice, DIO C57BL/6 mice, and DB mice) exhibited a statistically significant inverse relationship with blood HbA1c ($R = -0.84$, $P < 0.001$; Fig. 1A). We also showed that plasma AKG levels in DIO and DB mice were significantly lower than levels in chow mice (Fig. 1B). Notably, we showed that AKG concentration exhibited a similar inverse relationship with HbA1c levels in human plasma ($R = -0.39$, $P = 0.01$; Fig. 1C). Conversely, the concentrations of AKG-related metabolites, including glutamine ($R = 0.23$, $P = 0.09$), α-ketoisovaleric acid ($R = 0.33$, $P < 0.05$), succinic acid ($R = 0.35$, $P < 0.05$), α-ketoleucine ($R = 0.47$, $P < 0.01$), and fumaric acid ($R = 0.47$, $P < 0.01$), showed a positive relationship with HbA1c levels in human plasma (Fig. 1D). Collectively, blood AKG is negatively associated with glycemia, suggesting a physiological role in glycemic control.

AKG treatment improves glucose homeostasis

The negative correlation between circulating AKG levels and glycemia prompted us to investigate the role of AKG in glycemic control. Specially, ad libitum chow-fed or HFD-fed male C57BL/6 mice were provided with drinking water supplemented with 2% AKG. This dose of AKG supplementation significantly increased circulating AKG levels (fig. S1A), which were comparable to that observed in mice receiving resistance exercise, suggesting a physiological boost of circulating AKG (*7*). As the primary screening tests, we measured circulating glucose, HbA1c, insulin, and glucagon. While AKG supplementation failed to affect blood glucose in chow-fed mice (Fig. 2A), it significantly decreased glucose and HbA1c and

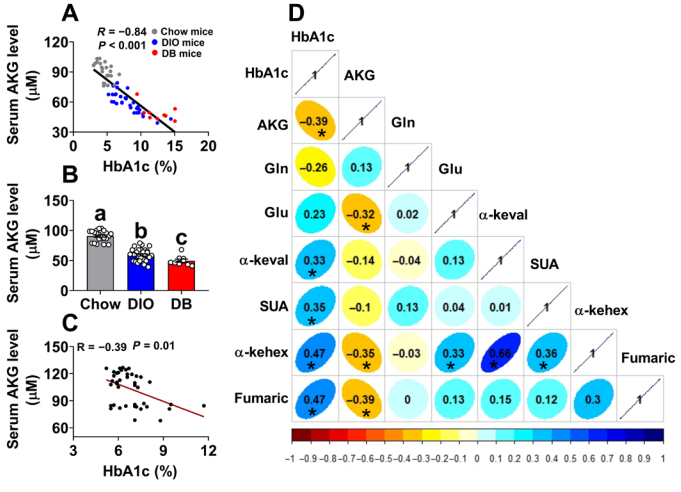

Fig. 1. Serum AKG level is negatively correlated with HbA1c. (**A**) Two-tailed Pearson's correlation coefficient analysis of plasma AKG level and HbA1c in mice. (**B**) Plasma AKG level in chow, DIO, and DB mice. Chow male mice were fed a chow diet at 8 weeks of age ($n = 22$). For DIO mice, 8-week-old male C57BL/6 mice were fed an HFD for 12 weeks ($n = 30$). DB (*db/db* diabetes) male mice were fed a chow diet at 10 weeks of age ($n = 9$). (**C**) Two-tailed Pearson's correlation coefficient analysis of plasma AKG level with HbA1c in Chinese adults (36 males and 6 females). (**D**) Two-tailed Pearson's correlation coefficient analysis of plasma AKG and related metabolite level with HbA1c in Chinese adults (36 males and 6 females). *$P < 0.05$ indicates significant correlation between human plasma AKG and related metabolite level with HbA1c. Gln, glutamine; Glu, glutamic acid; α-keval, α-ketoisovaleric acid; SUA, succinic acid; α-kehex, α-ketoleucine. Results are presented as means ± SEM. (A, C, and D) Two-tailed Pearson's correlation coefficient analysis. In (B), different letters between bars indicate $P \leq 0.05$ by one-way analysis of variance (ANOVA) followed by post hoc Tukey's tests.

increased insulin without changing glucagon in the blood of HFD-fed mice (Fig. 2, B to E). Notably, in these HFD-fed mice, AKG also decreased body weight and fat mass but increased lean mass without changing food intake (fig. S1, B and C), which is consistent with our previous observations (*7*). We also found that AKG supplementation effectively decreased the nonesterified fatty acid (NEFA) levels and triglyceride (TG) content in both plasma and liver (fig. S1, E to H) and reduced hepatic lipid accumulation (fig. S1I). AKG supplementation also increased mitochondrial DNA content, as indicated by up-regulated gene expression of cytochrome b (fig. S1J), and enhanced mitochondrial energy metabolism, as indicated by increased gene expression of the mitochondrial transcription factor A (*Tfam*), adenosine triphosphate (*ATP*) synthase H^+ transporting mitochondrial F1 complex β subunit (*Atp5b*), and succinate dehydrogenase (*SDH*) (fig. S1K). These results suggest a potential role of mitochondria in AKG's effects on hepatic glucose metabolism.

To further characterize the glucose homeostasis phenotype, glucose tolerance tests (GTTs), insulin tolerance tests (ITTs), and pyruvate tolerance tests (PTTs) were performed. While AKG failed to change glucose tolerance (Fig. 2F), it increased insulin tolerance (Fig. 2G) and pyruvate tolerance (Fig. 2H). Notably, increased insulin was also observed in AKG-treated mice after pyruvate challenge (Fig. 2I). Subsequently, we used hyperinsulinemic-euglycemic clamp to further evaluate insulin sensitivity. Consistently, we found that AKG significantly increased the whole-body insulin sensitivity, demonstrated by elevated glucose infusion rate (Fig. 2J). Glucose disposal rate (reflecting glucose disposal primarily in the muscle and adipose tissue) was not affected by AKG treatment (Fig. 2K). We further analyzed endogenous glucose productions (EGPs; largely resulting from hepatic glucose production) at the basal and clamped conditions. The basal EGP was comparable between control and AKG-treated mice. Under the clamped condition, AKG induced a robust and significant reduction in EGP (Fig. 2L). Therefore, AKG-induced glycemia-lowering effects are likely explained by increased pancreatic insulin secretion and an improvement in insulin sensitivity and hepatic insulin action.

To further characterize the hepatic glucose phenotypes induced by chronic AKG supplementation, we analyzed the hepatic expression of rate-limiting enzymes involved in gluconeogenesis, glycogenesis, glycolysis, and pentose phosphate pathway (PPP). Consistent with the results from PTT and clamp studies, we found that AKG markedly decreased the expression and activity of gluconeogenesis-related enzymes, including phosphoenolpyruvate carboxykinase (*PEPCK*), glucose 6-phosphatase (*G6Pase*), and fructose 1,6-bisphosphatase (*FBP*) (Fig. 2, M to P). Our data also showed that AKG supplementation inhibited the glycolysis pathway as indicated by decreased mRNA expression of phosphofructokinase (*Pfkl*), aldolase fructose-bisphosphate A (*Aldoa*), and lactate dehydrogenase A (*Ldha*) (fig. S1L). Besides, AKG also suppressed the PPP and glycogenesis pathway as shown by down-regulated mRNA levels of glycerate kinase (*Glyctk*), fructose-bisphosphatase 1 (*FBP1*), phosphodiesterase 1 (*Enpp1*), glycogen synthase 2 (*Gys2*), and acyl-CoA (coenzyme A) dehydrogenase (*Acadm*), as well as by up-regulated mRNA levels of fructose-bisphosphate C aldolase (*Aldoc*) (fig. S1L). While AKG supplementation increased the storage of glucose (glycolysis, pentose phosphate, and glycogenesis), it also reduced the source of glucose (gluconeogenesis), which ultimately leads to lower blood glucose levels. Together, our data suggest that chronic AKG supplementation improves hepatic glucose metabolism.

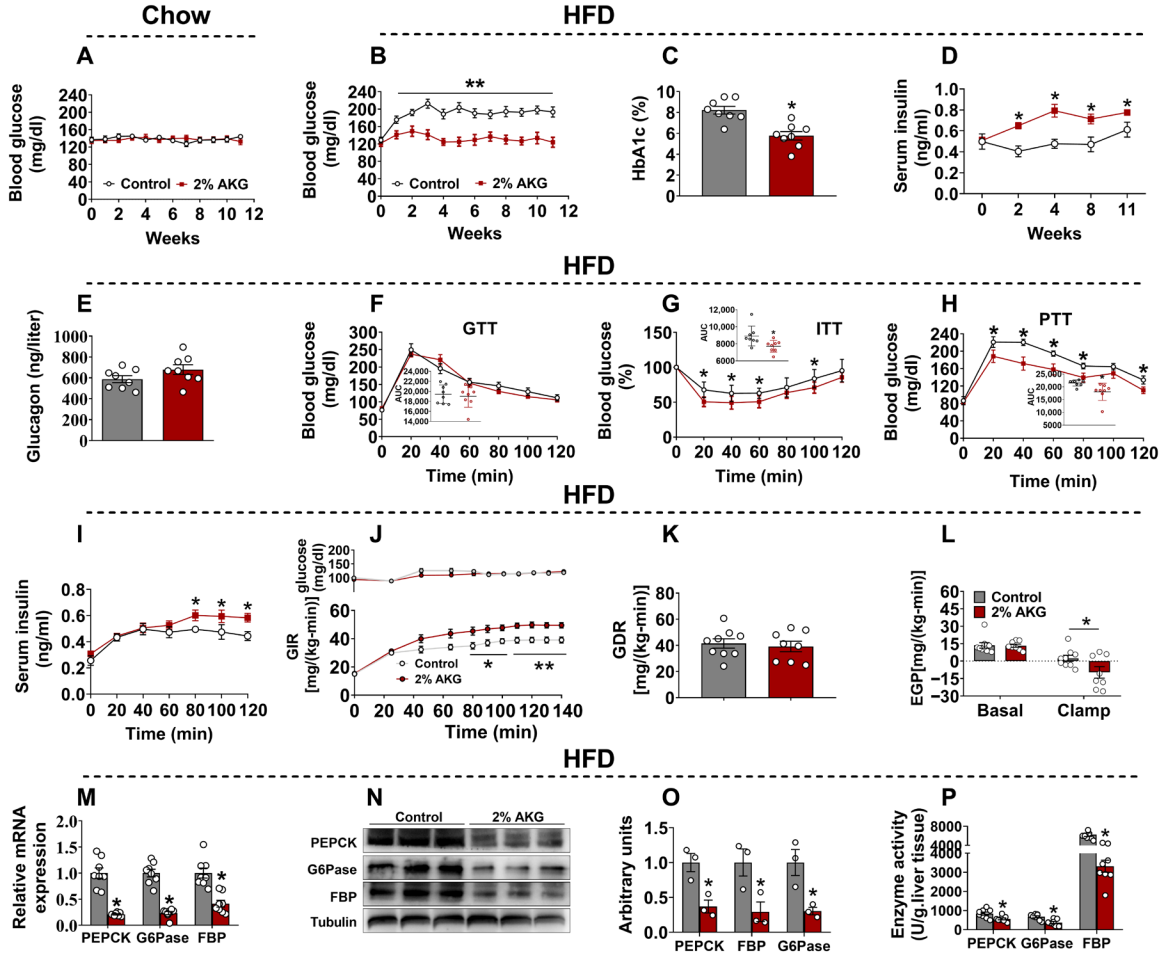

Fig. 2. Chronic AKG supplementation prevents diet-induced hyperglycemia. (**A**) Blood glucose from chow-fed mice supplemented with 2% AKG for 11 weeks ($n = 8$). (**B** to **E**) Blood glucose (B), serum HbA1c level (C), insulin level (D), and glucagon level (E) from HFD-fed mice supplemented with 2% AKG for 11 weeks ($n = 8$). (**F** to **H**) GTT (1 g/kg) (F), ITT (1 U/kg) (G), and PTT (1 g/kg) (H) in HFD-fed mice ($n = 8$). (**I**) Serum insulin level during PTT (1 g/kg) ($n = 8$). (**J** to **L**) Time course of blood glucose and glucose infusion rate (GIR) during hyperinsulinemic-euglycemic clamping (Clamp) (J), glucose disposal rate (GDR) (K), and endogenous glucose production (EGP) (L) from HFD-fed mice supplemented with 2% AKG for 11 weeks ($n = 8$ to 9). (**M** to **P**) mRNA expression (M), immunoblots (N) and quantification (O), and enzyme activity (P) of PEPCK, G6Pase, and FBP in the mice liver ($n = 8$). Results are presented as means ± SEM. (A, B, D, and F to J) $^*P \leq 0.05$ by two-way ANOVA followed by post hoc Bonferroni tests. (C, E, K to M, O, and P) $^*P \leq 0.05$ by nonpaired Student's *t* test.

Glycemia-lowering effect of AKG is mediated by suppression of hepatic gluconeogenesis

Since both anti-obesity and glycemia-lowering effects were observed after chronic AKG supplementation, it is likely that improved glucose homeostasis is partially attributed to body weight loss. To investigate whether AKG has direct anti-hyperglycemia effects, we examined the glycemic effects of single-bolus AKG injection in weight-matched HFD-fed male C57BL/6 mice. Specifically, mice were intraperitoneally injected with AKG at a dose of 10 mg/kg. This dose of AKG treatment has been shown to increase circulating AKG concentration (Fig. 3A), which is up to a comparable level observed after chronic 2% AKG water supplementation. The result showed that AKG-treated mice exhibited lower blood glucose at 1, 2, and 3 hours after injection compared with saline-treated mice (Fig. 3B). Notably, AKG administration also increased plasma insulin levels at 2 and 3 hours after injection (Fig. 3C). Similar decreases in hepatic mRNA expression, protein expression, and activities of PEPCK, G6Pase, and FBP were also observed (Fig. 3, D and F to H). Rapid reduction of mRNA expression prompted us to test whether AKG regulates gluconeogenesis protein in a transcriptional way. Specifically, we cotreated AKG with actinomycin D, an effective transcriptional inhibitor (*11*), to inhibit mRNA transcription (Fig. 3E). We found that AKG administration failed to affect the mRNA expression of PEPCK, G6Pase, and FBP (Fig. 3E), compared with actinomycin D–treated mice. These results suggest that AKG inhibits hepatic gluconeogenesis via a transcriptional way.

Consistently, the direct glycemic effects of AKG were also observed in another widely used diabetic mouse model, DB mice (*12*). We found that acute AKG treatment significantly decreased blood glucose (fig. S2A), hepatic gluconeogenesis protein expression, and enzyme activities (fig. S2, B to D), as well as increased serum insulin levels (fig. S2E) in weight-matched male DB mice. These results indicate that, like chronic supplementation, acute intraperitoneal injection of AKG also inhibits hepatic gluconeogenesis and stimulates insulin secretion, supporting a direct effect of AKG on glucose homeostasis. In line with our observations that both chronic and

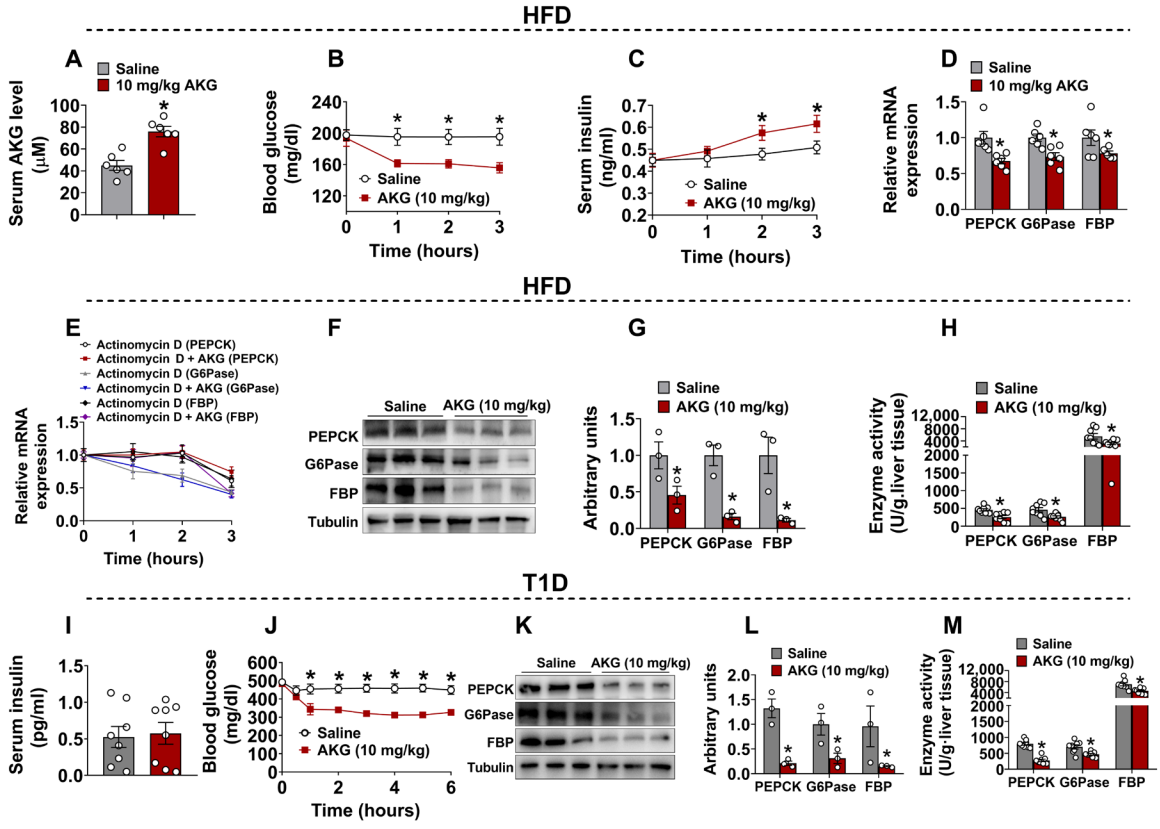

Fig. 3. Acute AKG administration prevents diet-induced hyperglycemia in HFD mice and T1D diabetic mice. (**A** to **C**) Serum AKG level (A), blood glucose level (B), and insulin level (C) in male C57BL/6 mice (12 weeks old) fed with HFD intraperitoneal saline or AKG (10 mg/kg body weight) for 3 hours ($n = 6$ to 8). (**D**) PEPCK, G6Pase, and FBP mRNA expression in mice liver ($n = 6$). (**E**) PEPCK, G6Pase, and FBP mRNA expression in the liver. Mice (12 weeks old) fed with HFD intraperitoneal actinomycin D (1 mg/kg) or actinomycin D (1 mg/kg) + AKG (10 mg/kg) for 1, 2, and 3 hours ($n = 6$). (**F** to **H**) Immunoblots (F) and quantification (G), and enzyme activity (H) of PEPCK, G6Pase, and FBP in mice liver ($n = 3$ to 8). (**I** and **J**) Serum insulin level (I) and blood glucose (J) in T1D male mice (12 weeks old) fed with chow diet intraperitoneal saline or AKG for 6 hours ($n = 8$). (**K** to **M**) Immunoblots (K) and quantification (L), and enzyme activity (M) of PEPCK, G6Pase, and FBP in mice liver ($n = 3$ to 8). Results are presented as means ± SEM. (B, C, E, and J) $^*P \leq 0.05$ by two-way ANOVA followed by post hoc Bonferroni tests. (A, D, G to I, L, and M) $^*P \leq 0.05$ by nonpaired Student's *t* test.

acute AKG treatment increased insulin release (Figs. 2D and 3C), AKG has been recently found to act as a metabolic signaling molecule to regulate pancreatic β cell function and promote insulin secretion (*13*). We speculated that AKG-induced hyperinsulinemia is the major factor responsible for the glucose-lowering effects of AKG. To test the requirement of insulin, we investigated AKG's effects in a chemical-induced insulin-deficient T1D mouse model. Specifically, impairment of islet function and insulin secretion was induced by 7-day intraperitoneal injection of streptozotocin (STZ) in male C57BL/6 mice. Compared to intact mice (insulin level, ~0.5 ng/ml; Fig. 3C), STZ-treated mice exhibit significantly lower serum insulin levels (0.2 to 0.5 pg/ml), which were not changed by AKG treatment (Fig. 3I). These findings suggested impaired insulin secretion and verified our T1D mouse model. Unexpectedly, we found that impaired insulin secretion did not block the regulatory effects of AKG on glucose homeostasis, as indicated by decreased blood glucose levels (Fig. 3J), and decreased hepatic protein expression and enzyme activities of PEPCK, G6Pase, and FBP (Fig. 3, K to M). Moreover, we also fed this T1D mouse model with an HFD. The results showed that AKG administration still decreased blood glucose levels at 2 and 3 hours after intraperitoneal injection of AKG (fig. S2F). Notably, similar inhibitory effects were found on the protein expression and enzyme activities of PEPCK, G6Pase, and FBP (fig. S2, G to I). These results indicate that the glycemia-lowering effects of AKG are at least partially mediated by an insulin-independent mechanism.

AKG directly inhibits hepatic gluconeogenesis in an OXGR1-independent mechanism

As an important signal molecule in organism, AKG regulates physiological progress by acting on related target organs, such as adipose tissue, intestinal, brain, and muscle (*14*). We next asked whether decreased hepatic gluconeogenesis induced by AKG results from a direct effect on the liver. We examined the effects of AKG treatment in in vitro primary hepatocyte or ex vivo liver slice culture model. To induce an insulin resistance hepatic cell model, primary hepatocyte obtained from chow-fed male C57BL/6 mice was treated with 0.25 mM palmitic acid (PA) for 24 hours (*15*). We found that 0.25 mM PA effectively increased hepatocyte glucose production (HGP) (Fig. 4B). Notably, in control primary hepatocytes without PA treatment, 100 μM AKG treatment failed to affect HGP or protein expression and the enzyme activities of PEPCK, G6Pase, and FBP. Conversely, in PA-treated primary hepatocytes, AKG treatment significantly decreased the HGP as well as protein expression and

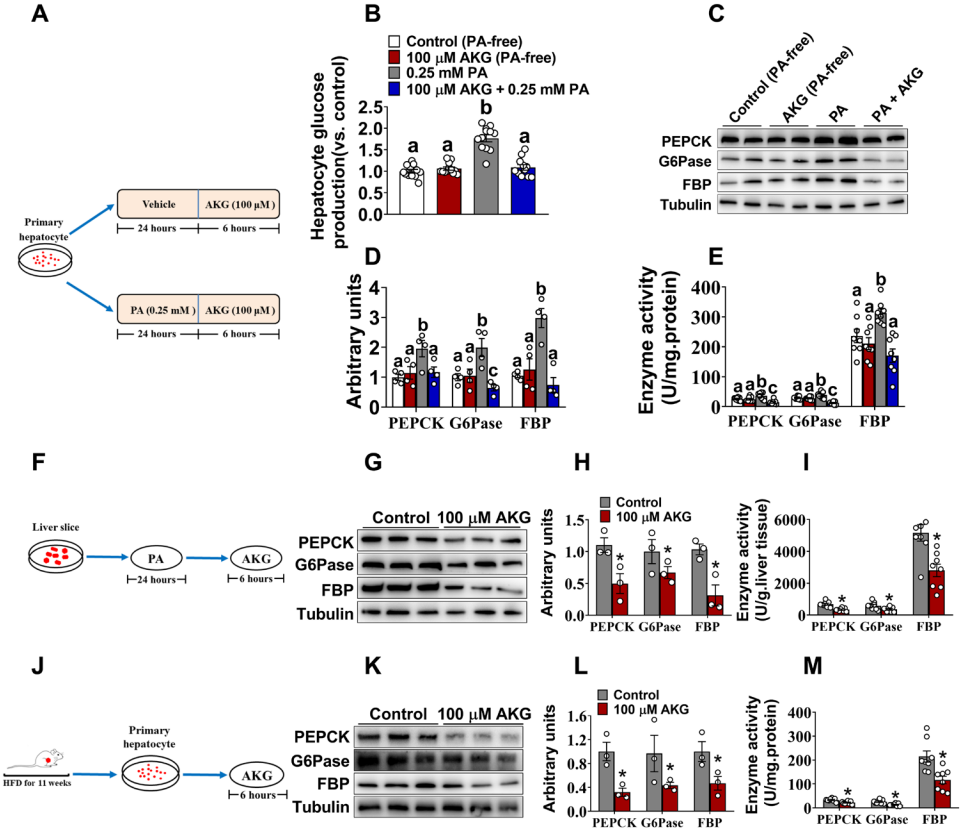

Fig. 4. AKG suppresses hepatic gluconeogenesis in vitro. (**A**) Schematic representation of primary hepatocyte treated with AKG. (**B** to **E**) Basal glucose production (B), immunoblots (C) and quantification (D), and enzyme activity (E) of PEPCK, G6Pase, and FBP from 12-week-old male C57BL/6 mouse primary hepatocyte cultured with vehicle or 0.25 mM PA for 24 hours and then treated with vehicle or 100 μM AKG for 6 hours ($n = 4$ to 12). (**F**) Schematic representation of liver slice treated with AKG. (**G** to **I**) Immunoblots (G) and quantification (H), and enzyme activity (I) of PEPCK, G6Pase, and FBP. Liver slices were cultured with 0.25 mM PA for 24 hours and then treated with vehicle or 100 μM AKG for 6 hours ($n = 3$ to 8). (**J**) Schematic representation of primary hepatocyte treated with AKG. (**K** to **M**) Immunoblots (K) and quantification (L), and enzyme activity (M) of PEPCK, G6Pase, and FBP. Twelve-week-old male C57BL/6 mice were fed an HFD for 11 weeks. Primary hepatocytes were treated with vehicle or 100 μM AKG for 6 hours ($n = 3$ to 8). Results are presented as means ± SEM. In (B), (D), and (E), different letters between bars indicate $P \leq 0.05$ by one-way ANOVA followed by post hoc Tukey's tests. (H, I, L, and M) $^*P \leq 0.05$ by nonpaired Student's *t* test.

activities of gluconeogenesis enzymes (Fig. 4, A to E). These data suggest a direct effect of AKG in in vitro primary hepatocyte. Consistently, we also found decreased protein expression and enzyme activities of PEPCK, G6Pase, and FBP in PA-treated liver slices (Fig. 4, F to I) and primary hepatocytes derived from DIO mice (Fig. 4, J to M). Thus, the results from both in vitro and ex vivo hepatic models supported a direct effect of AKG on hepatic gluconeogenesis.

OXGR1 has been identified as the primary mediating receptor for anti-obesity effects of AKG (*7*). *OXGR1* deletion blocked the inhibitory effects of chronic AKG supplementation on body weight, fat mass, and tissue index and size of gonadal white adipose tissue (gWAT), as well as stimulatory effects on tissue index and fiber size of gastrocnemius muscle (Fig. 5, A to G). Notably, OXGR1 deletion failed to affect AKG's effects on blood glucose, blood HbA1c level, insulin level, pyruvate tolerance, and hepatic protein expression and activity of PEPCK, G6Pase, and FBP (Fig. 5, H to O). These results suggest that OXGR1 is not required for glycemia-lowering effects of AKG.

Serpina1e is required for the suppressive effects of AKG on hepatic gluconeogenesis

To explore the mechanism of AKG-induced gluconeogenesis suppression, we investigated the transcriptomic alteration induced by chronic AKG treatment in the liver of DIO mice. We found that multiple genes showed profound transcriptional changes (Fig. 6, A and B). These genes included *serpina1e*, encoding a protein called α1-antitrypsin, which is a type of serine protease inhibitor (*16*); selenium binding protein 2 (*selenbp2*), which had been identified as the major target for acetaminophen in the liver (*17*); cytochrome P450, family 2, subfamily c, polypeptide 70 (*cyp2c70*), which regulates the hydroxylated muricholic acid formation (*18*); and cytochrome P450, family 4, subfamily a, polypeptide 12b (*cyp4a12b*), which conducts ω hydroxylation of fatty acids (*19*). All these genes are highly expressed in the liver and involved in liver metabolism.

To further test whether these genes are essential for AKG-induced suppression on hepatic gluconeogenesis, we generated in vitro loss-of-function primary hepatocyte models by using small interfering RNA (siRNA) to target *serpina1e*, *selenbp2*, *cyp2c70*, or *cyp4a12b*, respectively. We found that the siRNA-treated primary hepatocyte showed significantly lower mRNA or protein expression of targeted genes compared with control scrambled siRNA-treated cells (Fig. 6C and fig. S3, A, B, F, G, and K), thereby validating primary hepatocyte knockdown models. We showed that the knockdown of *serpina1e*, but not *selenbp2*, *cyp2c70*, and *cyp4a12b*, effectively abolished the inhibitory effects of AKG on the protein expression and activities of

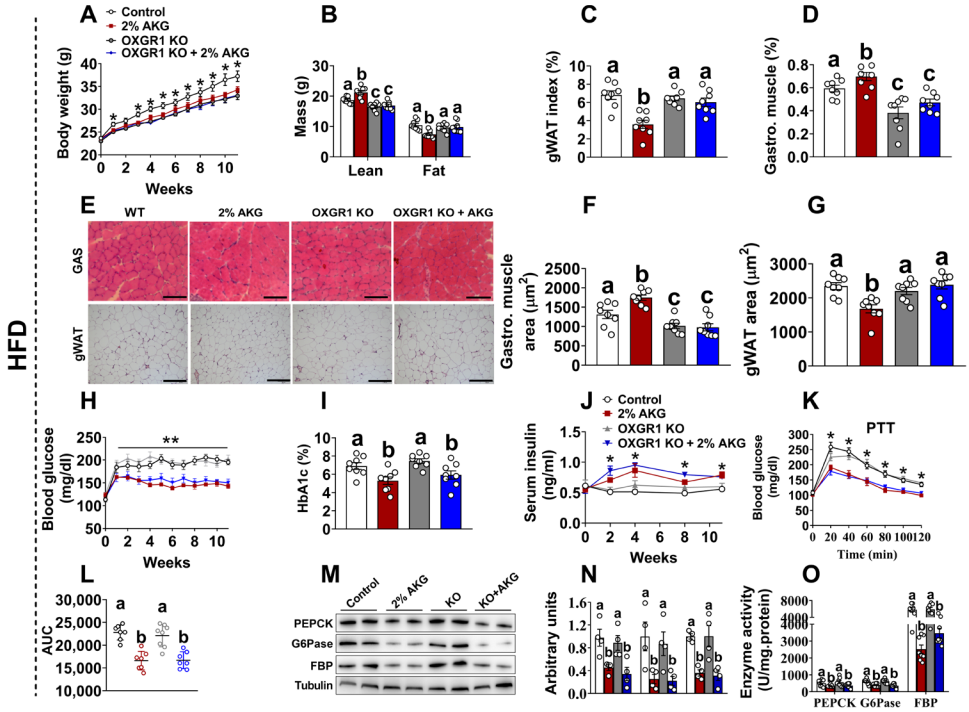

Fig. 5. OXGR1 is not required for AKG-induced gluconeogenesis suppression. (**A** to **D**) Body weight (A), body composition (B), gWAT index (C), and gastrocnemius (Gastro.) muscle index (D) of male wild-type (WT) control (littermates) or OXGR1KO mice. At 12 weeks of age, both control and knockout (KO) mice were switched to HFD and further divided into two groups, receiving tap water or water supplemented with 2% AKG for 11 weeks ($n = 8$). (**E** to **G**) Representative images (E) and quantification (F and G) of hematoxylin and eosin (H&E) staining in gWAT and gastrocnemius ($n = 8$). H&E staining shows the size of gastrocnemius fibers (F) and adipocytes (G). gWAT bar is 50 μm; gastrocnemius bar is 25 μm. (**H** to **L**) Blood glucose (H), serum HbA1c level (I), insulin level (J), and PTT (K and L) ($n = 8$). (**M** to **O**) Immunoblots (M) and quantification (N), and enzyme activity (O) of PEPCK, G6Pase, and FBP ($n = 4$ to 8). Results are presented as means ± SEM. (A, H, J, and K) *$P \leq 0.05$ by two-way ANOVA followed by post hoc Bonferroni tests. In (B) to (D), (F), (G), (I), (L), (N), and (O), different letters between bars indicate $P \leq 0.05$ by one-way ANOVA followed by post hoc Tukey's tests.

PEPCK, G6Pase, and FBP in PA-treated primary hepatocyte (Fig. 6, D to F, and fig. S3, C to E, H to J, and L to N), suggesting a vital role of serpina1e in AKG-induced hepatic gluconeogenesis.

In supporting this view, we found that the mRNA expression of hepatic serpina1e in DIO or DB mice is lower than that in chow-fed mice (Fig. 6G), suggesting the metabolic relevance of hepatic serpina1e. Consistently, we also showed that chronic AKG supplementation increased the protein expression of phosphorylation of focal adhesion kinase (FAK) (Fig. 6, H and I), a tyrosine-phosphorylated protein mediating the regulatory effects of serine protease inhibitors on cell physiological metabolism. As an important signaling pathway member of FAK, phosphorylation of Akt was also increased with AKG treatment (Fig. 6, H and I). In summary, our results suggest an essential role of serpina1e in AKG-induced inhibition on hepatic gluconeogenesis.

To further determine the role of serpina1e in the systemic effects of AKG on glucose homeostasis, we generated a serpina1e liver-specific knockout (KO) mouse model (Alb-serpina1e$^{-/-}$). Specifically, Alb-Cre mice were crossed with LSL-Cas9-EGFP mice to generate Alb-Cre/LSL-Cas9-EGFP (Alb-Cas9), a mouse model with Cas9 selectively overexpressed in Alb-positive liver cells. Subsequently, a liver-specific adeno-associated virus (AAV) harboring single-guide RNAs (sgRNAs) targeting serpina1e or scramble sgRNAs was intravenously injected to generate serpina1e-deficient mice or control mice, respectively. We found that the Alb-serpina1e$^{-/-}$ mice showed decreased serpina1e mRNA expression in the liver compared with the control mice (Fig. 6J), which validates our KO model. Consistent with the in vitro primary hepatocyte model, liver-specific serpina1e KO abolished the AKG-induced decreases of blood glucose (Fig. 6K), PTT (Fig. 6L), and inhibition on hepatic gluconeogenesis as indicated by the protein expression and activities of PEPCK, G6Pase, and FBP (Fig. 6, N to P). Conversely, liver-specific serpina1e KO failed to disrupt the effects of acute AKG treatment on plasma insulin secretion (Fig. 6Q) and ITT (Fig. 6M). Besides, liver-specific serpina1e KO had no effect on mice body weight or body weight gain when fed HFD (fig. S4, A and B). Collectively, these findings support a model that AKG acts on hepatic serpina1e signaling to reduce gluconeogenesis and glycemia.

To further determine the role of liver serpina1e in hepatic gluconeogenesis, we generate liver-specific overexpression mouse model (Serpina1e^{OE}). In this model, the HBAAV8-serpina1e virus was delivered into the liver of wild-type (WT) mice. The mRNA of serpina1e was successfully overexpressed in the liver of serpina1e^{OE} mice compared to WT mice injected with HBAAV8-GFP (green fluorescent protein) control virus (fig. S5A). We found that liver overexpression of serpina1e decreased blood glucose and gluconeogenesis as indicated by mRNA and protein expression of PEPCK, G6Pase, and FBP (fig. S5, B to E), but not insulin (fig. S5F). Thus, the results from both loss-of-function and gain-of-function models demonstrated that serpina1e mediates the liver gluconeogenesis progress.

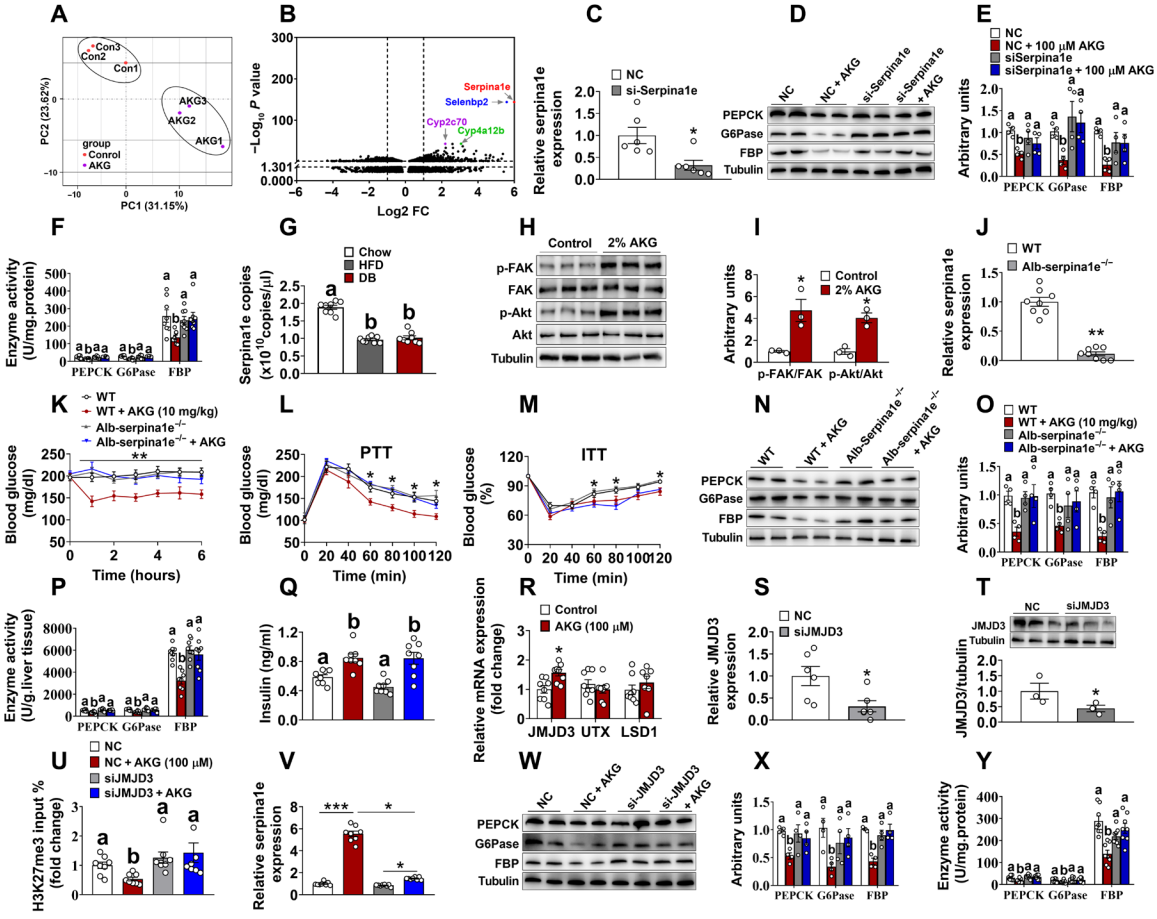

Fig. 6. *Serpina1e* is required for the inhibitory effects of AKG on hepatic gluconeogenesis. (**A** and **B**) Principal coordinate analysis plot (A) and volcano plot of AKG-induced transcriptome signature (B) ($n = 3$). (**C**) mRNA expression of serpina1e in si-serpina1e–treated primary hepatocyte ($n = 6$). (**D** to **F**) Immunoblots (D) and quantification (E), and enzyme activity (F) of PEPCK, G6Pase, and FBP in primary hepatocyte (PA treatment) ($n = 4$ to 8). (**G**) mRNA expression of serpina1e in the liver ($n = 8$). (**H** and **I**) Immunoblots (H) and quantification (I) of p-FAK and p-Akt protein expression in the liver ($n = 3$). (**J**) mRNA expression of serpina1e in Alb-serpina1e$^{-/-}$ mice liver ($n = 8$). (**K** to **M**) Blood glucose (K), PTT (L), and ITT (M) in Alb-serpina1e$^{-/-}$ mice ($n = 8$). (**N** to **P**) Immunoblots (N) and quantification (O), and enzyme activity (P) of PEPCK, G6Pase, and FBP in the liver ($n = 4$ to 8). (**Q**) Serum insulin level ($n = 8$). (**R**) mRNA expression of JMJD3, LSD1, and UTX in AKG-treated primary hepatocyte (PA treatment) ($n = 8$). (**S** and **T**) mRNA (S) and protein (T) expression of JMJD3 in si-JMJD3–treated primary hepatocyte ($n = 3$ to 6). (**U**) Chromatin immunoprecipitation analysis of H3K27me3 in promoter of serpina1e in si-JMJD3–treated primary hepatocyte (PA treatment) ($n = 8$). (**V**) mRNA expression of serpina1e in si-JMJD3–treated primary hepatocyte (PA treatment) ($n = 8$). (**W** to **Y**) Immunoblots (W) and quantification (X), and enzyme activity (Y) of PEPCK, G6Pase, and FBP in si-JMJD3–treated primary hepatocyte (PA treatment) ($n = 4$ to 8). Results are presented as means ± SEM. In (E) to (G), (O) to (Q), (U), (X), and (Y), different letters between bars indicate $P \leq 0.05$ by one-way ANOVA followed by post hoc Tukey's tests. (C, I, J, R to T, and V) *$P \leq 0.05$ by nonpaired Student's *t* test. (K to M) *$P \leq 0.05$, **$P \leq 0.01$ by two-way ANOVA followed by post hoc Bonferroni tests.

The inhibitory effects of AKG on hepatic gluconeogenesis rely on JMJD3/H3K27me3/serpina1e pathway

The next question is how AKG regulates hepatic serpina1e expression and gluconeogenesis. Besides acting on the membrane receptor OXGR1, AKG also regulates metabolic processes through epigenetic modification (*20*). Serving as a vital substrate and cofactor for epigenetic modifications, including RNA methylation and histone methylation, AKG plays a vital role in beige adipose thermogenesis, macrophage orchestration, and mitochondrial glucose metabolism (*8*, *20*, *21*). It is possible that AKG increases hepatic serpina1e expression through epigenetic mechanisms. We first investigated AKG's effects on RNA m6A modification (N6-methyladenosine), which is the most prevalent RNA modification and has been reported in numerous human diseases, including several cancers (*22*). Our transcriptomic results showed that chronic AKG supplementation did not change the mRNA expression of three major types of enzymes involved in m6A methylation: writers, erasers, and readers (*22*) in the liver of DIO mice (fig. S6A). Specifically, these writers include methyltransferase-like 3 (*METTL3*), *METTL14*, Wilms' tumor 1–associating protein (*WTAP*), RNA binding motif protein 15 (*RBM15*), and zinc finger CCCH-type containing 13 (*ZC3H13*). Readers include YTH N6-methyladenosine RNA binding protein 1 (*YTHDF1*), *YTHDF2*, *YTHDF3*, YTH domain containing 1 (*YTHDC1*), *YTHDC2*, insulin-like growth factor 2 mRNA binding protein 2 (*IGF2BP2*), *IGF2BP3*, heterogeneous nuclear ribonucleoprotein A2/B1 (*HNRNPA2B1*), *HNRNPC*, and FMRP translational regulator 1 (*FMR1*). Erasers include FTO α-ketoglutarate–dependent dioxygenase (*FTO*) and ALKB homolog 5, RNA demethylase (*ALKBH5*). Consistently, AKG failed to affect the mRNA expression of these writers, readers, and erasers in PA-treated primary hepatocytes (fig. S6B), suggesting an alternative epigenetic mechanism.

Subsequently, we further tested AKG's effects on histone demethylase, which has been reported as an epigenetic drug target for metabolic disease, such as obesity, hepatosteatosis, and type 2 diabetes (*23*, *24*). We specifically detected the mRNA expression of Jumonji domain-containing protein 3 (*JMJD3*), lysine-specific demethylase 1 (*LSD1*), and lysine demethylase 6A (*UTX*), the most widely known histone demethylases. We found that AKG increased the mRNA expression of JMJD3 without affecting LSD1 and UTX in PA-treated primary hepatocytes (Fig. 6R). JMJD3 is a primary demethylase of H3K27me3, a repressive epigenetic mark that prevents gene expression (*25*). We wondered whether AKG increases hepatic serpina1e expression by promoting JMJD3-dependent demethylation of H3K27 on the promoters of serpina1e.

To test it, we generated JMJD3 knockdown cell lines by transfecting primary hepatocytes with a plasmid harboring siRNA targeting JMJD3 (si-JMJD3) (Fig. 6, S and T). Primary hepatocytes were transfected with negative control (NC) siRNA or si-JMJD3 for 24 hours. Then, we found that JMJD3 knockdown not only abolished inhibitory effects of AKG on H3K27me3 levels at the promoter of serpina1e (Fig. 6U) but also attenuated the stimulatory effect of AKG on serpina1e mRNA expression (Fig. 6V) in PA-treated primary hepatocytes. Notably, JMJD3 knockdown also blunted AKG-induced decreases in protein expression and enzyme activities of PEPCK, G6Pase, and FBP (Fig. 6, W to Y). Collectively, these results provided in vitro evidence to support a mediating role of JMJD3/H3K27me3/Serpina1e signaling in the inhibitory effects of AKG on hepatic gluconeogenesis.

P2RX4/SLC25A11 mediates the extramitochondrial transport of AKG

Our data support an OXGR1-independent intracellular machinery, which involves JMJD3/H3K27me3/serpina1e signaling in the nucleus. One obvious possible mechanism is through hepatocyte uptake of dietary AKG to modulate AKG-dependent histone epigenetic modification. However, it is well established that AKG does not cross plasma membranes (*26*). We replicated this finding in PA-treated hepatocytes. After treatment with ^{13}C-AKG for 24 hours, hepatocyte did not uptake any radiolabeled AKG (Fig. 7A), indicating that AKG is membrane impermeable in hepatocytes. Despite that exogenous AKG was not absorbed into the cells, intracellular total AKG levels were up-regulated by AKG incubation (Fig. 7B). Specifically, AKG levels in mitochondrial-free cytosol significantly increased, while AKG levels in mitochondrial tended to rise (Fig. 7, C and D), suggesting surface receptor/sensor-dependent modulation of mitochondrial-to-cytosol transportation of AKG.

While AKG is mainly generated in mitochondria, its levels outside the mitochondria vary substantially between cell types and fluctuate to regulate epigenetic modifications (*27*, *28*). We speculated that enhanced AKG transportation from mitochondria to cytosol mediates the regulatory effects of extracellular AKG on epigenetic modifications. The extramitochondrial AKG transport is mainly mediated by mitochondrial inner membrane proteins that transport small molecules between the cytosol and mitochondria (*29*). We first analyzed the transcriptomic expression of dicarboxylic acid transporters in the livers of AKG-treated male DIO mice. We found that AKG supplementation significantly increased the mRNA expression of solute carrier family 25 member 11 (*SLC25A11*) and sodium-dependent dicarboxylate cotransporter member 2 (*SLC13A2*) (Fig. 7E). SLC25A11 is a member of the malate-aspartate shuttle (MAS), regulating electroneutral exchange between AKG and other dicarboxylates (*30*), while SLC13A2 is the primary carrier involved in citrate reabsorption (*31*). Consistently, the protein expression of SLC25A11 was also increased by AKG treatment on the mitochondria membrane of PA-treated primary hepatocytes (Fig. 7F). To further test the requirement of SLC25A11 or SLC13A2, we generated SLC25A11 or SLC13A2 knockdown cell lines by transfecting primary hepatocytes with plasmid harboring siRNA targeting SLC25A11 or SLC13A2, respectively (Fig. 7G and fig. S6, C, E, and F). We found that knockdown of SLC25A11, but not SLC13A2, abolished AKG-induced hepatic gluconeogenesis suppression (Fig. 7, H to J, and fig. S6, G to I). Moreover, knockdown of SLC25A11 reversed the stimulatory effect of exogenous AKG on cytosol AKG (Fig. 7C). These in vitro data suggest that SLC25A11 is required for the regulatory effects of extracellular AKG on hepatic gluconeogenesis. These results support a model that dietary AKG enhances the hepatocyte mitochondrial membrane expression of SLC25A11 to increase cytosolic AKG levels, which subsequently stabilize the transcription of serpina1e through histone demethylation to inhibit hepatic gluconeogenesis.

One obvious missing part of this model is the surface protein that binds AKG to induce intracellular cascade. On the basis of the glycemic phenotypes of OXGR1 KO mice, it is unlikely to be OXGR1. OXGR1 shares high sequence homology with a family of purinoreceptors (*32*, *33*), suggesting a potential interaction between AKG and purinoreceptors. However, no evidence has been found to support a mediating role of purinoreceptors in AKG's functions.

Here, we found that chronic AKG supplementation significantly increased the mRNA expression of purinergic receptor *P2X4* (P2RX4) and decreased the mRNA expression of purinergic receptor P2Y2 (*P2RY2*) and purinergic receptor P2Y14 (*P2RY14*) (Fig. 7K), suggesting a possible involvement of these P2Y receptors. To test the possible interaction, we used surface plasmon resonance (SPR) to pull down all AKG-binding proteins and test the enrichment of these P2Y receptors (Fig. 7L). We found that P2RX4, but not P2RY2 or P2RY14, was enriched in AKG pull-down proteins when compared to running buffer pull-down controls (Fig. 7M), indicating a direct or indirect interaction between AKG and P2RX4. Here, we found that intraperitoneal injection of AKG (10 mg/kg) significantly increased AKG levels in mitochondrial-free cytosol with a tendency to raise AKG levels in mitochondrial (Fig. 7O). Notably, cotreatment of 5-(3-bromophenyl)-1,3-dihydro-2*H*-benzofuro[3,2-e]-1,4-diazepin-2-one (5-BDBD), a potent P2X4R antagonist (*34*), blunted these stimulatory effects induced by AKG (Fig. 7, N to O). To further investigate the requirement, we generated *P2RX4*, *P2RY14*, or *P2RY2* knockdown cell lines by transfecting primary hepatocytes with plasmid harboring siRNA targeting P2RX4, P2RY14, or P2RY2, respectively (Fig. 7P and fig. S6, D, J, K, O, and P). We found that knockdown of P2RX4, but not P2RY14 or P2RY2, abolished AKG-induced hepatic gluconeogenesis suppression (Fig. 7, Q to S, and fig. S6, L to N and Q to S). These data showed that P2RX4 might act as a surface AKG sensor to mediate the glycemic effects of AKG in hepatocytes.

DISCUSSION

The major finding of our study is that AKG, an exercise-induced myobolite (*35*), impairs hepatic gluconeogenesis and improves glucose homeostasis in diabetic mice. Our study revealed a negative

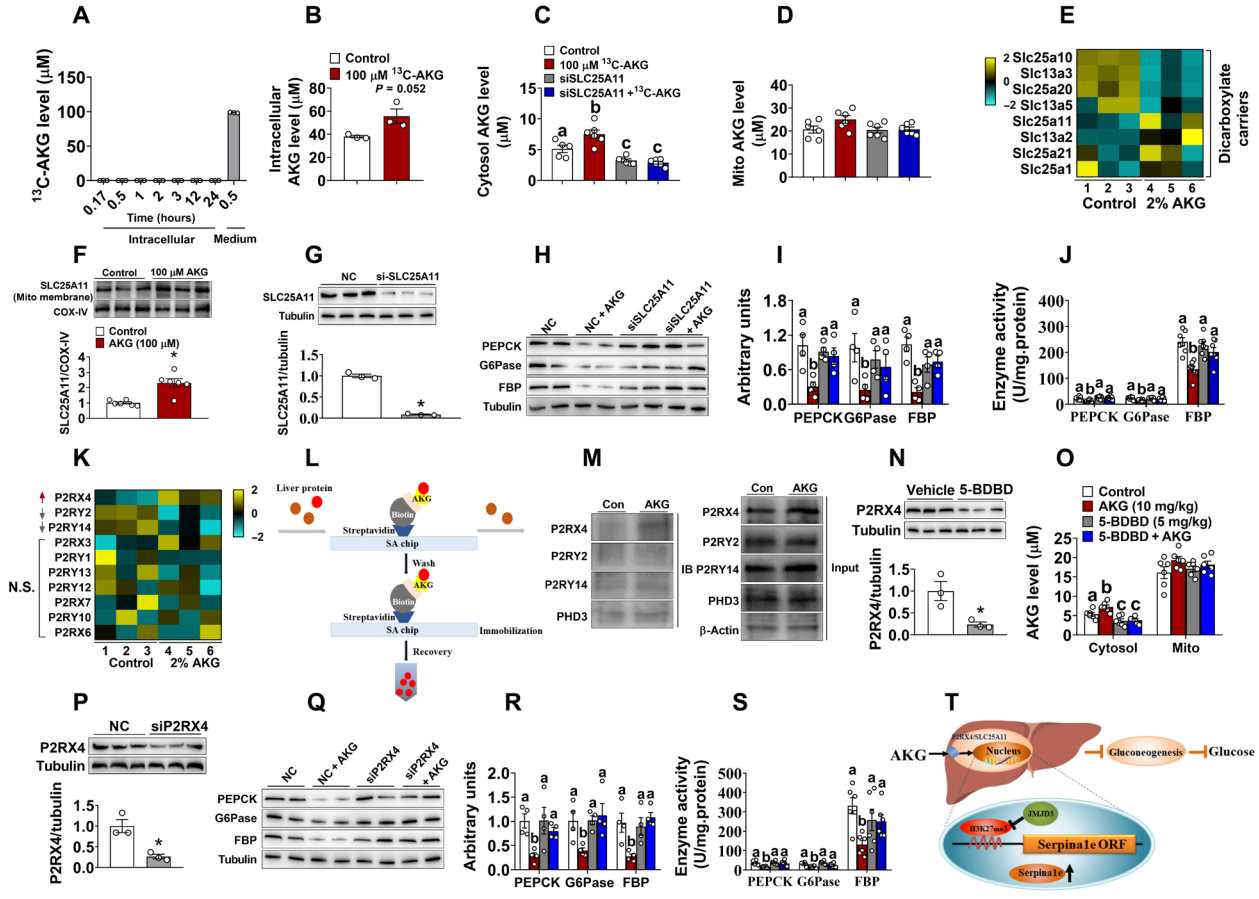

Fig. 7. P2RX4/SLC25A11 mediates the intracellular transport of AKG. (**A** and **B**) Intracellular and medium ^{13}C-AKG level (A) and intracellular total AKG level (B) ($n = 3$). (**C** and **D**) Cytosol (mitochondrial-free) (C) and mitochondrial (D) AKG level ($n = 6$). (**E**) Relative changes of dicarboxylate carriers in response to AKG treatment ($n = 3$). (**F**) SLC25A11 protein expression of mitochondrial membrane protein in AKG-treated primary hepatocytes (PA treatment) ($n = 6$). (**G**) Immunoblots of SLC25A11 in si-SLC25A11–treated primary hepatocyte ($n = 3$). (**H** to **J**) Immunoblots (H) and quantification (I), and enzyme activity (J) of PEPCK, G6Pase, and FBP in primary hepatocyte (PA treatment) ($n = 4$ to 8). (**K**) Relative changes of purine receptors in response to AKG treatment ($n = 3$). (**L**) Schematic representation of Biacore. (**M**) Immunoblots of protein expression after AKG pull-down in mice liver. (**N**) Immunoblots and quantification of P2RX4 in the liver. Twelve-week-old male mice were treated with vehicle or 5-BDBD (P2RX4 antagonist, 5 mg/kg) ($n = 3$). (**O**) Cytosol (mitochondrial-free) and mitochondrial AKG level ($n = 6$ per group). (**P**) Immunoblots and quantification of P2RX4 in si-P2RX4–treated primary hepatocyte ($n = 3$). (**Q** to **S**) Immunoblots (Q) and quantification (R), and enzyme activity (S) of PEPCK, G6Pase, and FBP in si-P2RX4–treated primary hepatocyte (PA treatment) ($n = 4$ to 8). (**T**) Graphic abstract mechanism of AKG on gluconeogenesis. Results are presented as means ± SEM. (B, F, G, N, and P) *$P \leq 0.05$ by nonpaired Student's t test. In (C), (D), (I), (J), (O), (R), and (S), different letters between bars indicate $P \leq 0.05$ by one-way ANOVA followed by post hoc Tukey's tests.

correlation between AKG and glucose in the blood of both humans and mice. Long-term systemic treatment of AKG effectively lowered blood glucose levels, which were associated with decreased hepatic gluconeogenesis and increased insulin secretion, in DIO and DB mice. Notably, the inhibitory effects of AKG on glycemia and hepatic gluconeogenesis were preserved in STZ-treated T1D and OXGR1KO mice, indicating an insulin- and OXGR1-independent mechanism. We also find that acute administration of AKG induced similar glucose responses as observed in mice chronically treated with AKG. Last, we provided in vitro, ex vivo, and in vivo evidence to support that AKG directly acts on *P2RX4/JMJD3/H3K27me3/serpina1e* pathway to inhibit hepatic gluconeogenesis and decrease blood glucose. Collectively, we provided a previously unidentified mechanism by which AKG inhibits hepatic gluconeogenesis and ameliorates hyperglycemia in diabetic mice.

Our results showed that chronic AKG treatment improved glucose homeostasis primarily by inhibiting hepatic gluconeogenesis without changing glucose tolerance in 3-month-old male DIO C57BL/6 mice. A similar beneficial effect of AKG on glucose balance was consistently reported in 10-month-old female DIO C57BL/6 mice (*8*). Specifically, while AKG treatment improved whole-body glucose tolerance, it failed to affect baseline blood glucose and insulin levels in these middle-aged female DIO mice (*8*). This discrepancy suggests an age- and sex-dependent glucose response to AKG treatment. It appears that glycemia-lowering effects of AKG decay during the aging process. The anti-obesity effects of AKG have been consistently shown by our group and others (*8*, *36*). It is possible that the glycemia-lowering effect of AKG is a secondary response to decreased adiposity. However, in this study, we provided multiple lines of evidence to support a distinct mechanism for AKG's effects on glucose homeostasis. First, we found that plasma AKG levels in nondiabetic obese mice are significantly higher than those in diabetic obese mice with similar body weight. This evidence suggests that the association between AKG and blood glucose is independent of body weight. Second, acute AKG treatment produce similar glycemia-lowering effects as observed in DIO and DB mice chronically

treated with AKG. Last, our previous observations found that AKG reduces obesity in an OXGR1-dependent mechanism (*8*, *36*). Specifically, compared to water-treated WT littermates, water-treated OXGR1 KO mice showed muscle hypotrophy and body weight loss when fed on HFD, suggesting a potential protective effect of OXGR1 on HFD-induced muscle loss. Notably, previously, we showed that HFD significantly decreased baseline circulating AKG level in mice (*7*), indicating that OXGR1 protects HFD-induced muscle loss when circulating AKG is low. The protective effect of OXGR1 is possibly mediated by directly decreasing muscle protein degradation (*37*). Besides, compared to water-treated WT mice, AKG-treated WT mice showed increased lean mass and decreased fat mass, resulting in reduced body weight. Conversely, the regulatory effects of AKG on lean mass, fat mass, and body weight were blocked in OXGR1 KO mice, suggesting a mediating role of OXGR1. It appears that OXGR1 only exerts beneficial effects on metabolic health and particularly muscle hypertrophy and fat loss when circulating AKG is high. However, OXGR1KO did not affect AKG's inhibitory effects on glycemia and hepatic gluconeogenesis in DIO mice, suggesting an OXGR1-independent mechanism. Collectively, AKG-induced glycemia-lowering effect is independent of its anti-obesity effect.

One interesting glucose phenotype is that both acute and chronic AKG treatments increase blood insulin but not glucagon levels in DIO and DB mice. These findings are consistent with previous reports that AKG stimulates insulin secretion through hypoxia-inducible factor–prolyl hydroxylases (*PHDs*) in clonal β cells as well as rodent and human islets (*13*, *38*). In addition, extracellular treatment of dimethyl AKG, a membrane-permeable AKG analog, has been shown to stimulate insulin secretion from isolated pancreatic islets at a stimulatory glucose concentration (*39*). Mechanistically, the stimulation of insulin secretion by extracellular dimethyl AKG partially depends on the direct inhibition of β cell K(ATP) channels. In addition, dimethyl AKG is also metabolized into AKG by ester cleavage after being absorbed intracellularly. The intracellular AKG further contributes to the stimulation of insulin secretion both by indirect K(ATP) channel inhibition (via activation of ATP production) and by an amplifying effect (*39*). These findings suggest a PHD/K(ATP) channel–mediated stimulatory effect of AKG on insulin secretion. Insulin was the primary hormone to regulate glucose homeostasis. Here, we found that AKG treatment decreased mice blood glucose at 1 hour in HFD model, while AKG decreased HFD + T1D mice blood glucose at 2 hours, which suggested that HFD + T1D partially block AKG's effects on glucose and gluconeogenesis. These results indicate the contribution from insulin. Collectively, while insulin contributes to some of the glucose phenotypes, some of AKG's effects are independent from insulin. Glucose-induced secretion of insulin is well known to inhibit hepatic glucose production (*40*), suggesting a possibility that AKG increases insulin secretion to indirectly inhibit hepatic gluconeogenesis. However, evidence from two separate mouse models implies an alternative mechanism. Specifically, depletion of endogenous insulin by STZ treatment did not affect AKG's effects on blood glucose and hepatic gluconeogenesis, suggesting an insulin-independent mechanism. In line with these observations, in liver-specific serpina1e KO mice, while the stimulatory effects on blood insulin levels persisted, the inhibitory effects of AKG on blood glucose and hepatic gluconeogenesis were abolished. Therefore, the glycemia-lowering effect of AKG does not rely solely on insulin secretion.

Glucose homeostasis is a dynamic process maintained through glucose consumption in metabolic tissues and production in the liver (*41*). In mammals, liver is the most important organ to regulate body glucose metabolism through glycolysis, PPP, and gluconeogenesis. Hepatic gluconeogenesis is an essential therapeutic target for T2DM. Several commercial available drugs, including metformin (*42*) and pioglitazone (*43*), effectively improve glucose homeostasis by acting on gluconeogenesis. Here, we found that chronic AKG treatment effectively inhibited mRNA expression of genes involved in glycolysis, pentose phosphate, and glycogen metabolism in the liver of DIO mice, suggesting the reduced glucose utilization. Moreover, AKG supplementation significantly suppressed the mRNA expression of gluconeogenesis gene, suggesting the increased glucose source. Consistently, chronic AKG treatment also improved pyruvate tolerance and inhibited the protein expression and activities of rate-limiting enzymes for gluconeogenesis. Like chronic treatment, acute AKG administration also suppressed essential gluconeogenesis enzyme activities and protein expression in in vivo DIO, T1D, and DB mouse models as well as in vitro primary hepatocyte and ex vivo liver slice. Moreover, we found that acute AKG treatment also effectively reduced hepatic glucose production in hepatocyte with 0.25 mM PA. Collectively, AKG generates a robust direct inhibition on hepatic gluconeogenesis. Numerous studies have established the pivotal role of liver-enriched transcriptional regulation in organ development and cellular metabolism, and conclusive evidence for liver transcription that the timely expression of transcription related gene expression is necessary for cellular differentiation or metabolism (*44*). Here, we showed that cotreated AKG with actinomycin D, an effective transcriptional inhibitor to inhibit mRNA transcription, failed to affect the mRNA expression of *PEPCK*, *G6Pase*, and *FBP* compared with actinomycin D–treated mice, suggesting a transcriptional way of AKG in hepatic gluconeogenesis regulation. Collectively, given the contribution of insulin in AKG-induced glucose suppression, we suspected that likely the acute effects are mediated through increased insulin and chronic effects are partially mediated by hepatic gluconeogenesis.

To explore the potential mechanisms for AKG's effects on hepatic gluconeogenesis, we screened transcriptomic changes induced by AKG treatment in the livers of DIO mice. We identified serpina1e, a member of serine protease inhibitors (serpins), as an AKG-induced transcriptomic signature. Serpins are the largest and most broadly distributed superfamily of protease inhibitors, and Serpina1 is highly expressed in the liver (*16*, *45*). To explore the role of serpina1e in hepatic gluconeogenesis, we generated a liver-specific overexpression of serpina1e mouse model (serpina1e^{OE}). We found that serpina1e overexpression effectively decreased gluconeogenesis enzymes' mRNA and protein expression, suggesting inhibitory effects of serpina1e on hepatic gluconeogenesis. Consistent with our observations, FAK, one of serpina1e's downstream effectors, has been shown to regulate glucose metabolism and liver disease (*46*, *47*). As important downstream signaling of FAK, the Akt pathway had been well known to inhibit hepatic gluconeogenesis in both in vitro hepatocytes and in vivo type 2 diabetic mice (*48*). On the basis of these findings, we speculate that the serpina1e/FAK/Akt pathway plays a vital role in the regulation of hepatic gluconeogenesis. It is possible that serpina1e mediates the inhibitory effects of AKG on hepatic gluconeogenesis and blood glucose. To directly test it, we generated a serpina1e knockdown primary hepatocyte model and liver-specific serpina1e-KO mouse model. In supporting our hypothesis, serpina1e

knockdown or KO effectively abolished AKG's effects on hepatic gluconeogenesis. These results reveal a potential role of AKG/serpina1e signaling in hepatic gluconeogenesis regulation.

Emerging evidence demonstrates that AKG serves as a signal molecule integrating metabolism and aging process by reducing epigenetic age in both humans and animals. Specifically, AKG regulates the function of essential enzymes that influence epigenetic modifications to modulate gene expression and intracellular metabolic process. These enzymes include 2-oxoglutarate-dependent demethylase (FTO), which is involved in RNA demethylation, and the JMJD family, which is the major histone demethylases (*49*, *50*). The epigenetic modifications induced by these two enzymes have been linked to metabolic disease. For example, N6-methyladenosine (m6A) methylation, one of the most common RNA modifications, plays a vital role in cancer therapy (*51*), obesity, and glucose metabolism (*52*). Similarly, liver-specific inhibition of JMJD3 and UTX increased H3K27me3 content and caused insulin intolerance and glucose disorder (*23*, *53*). On the basis of these reports, we speculate that AKG regulates serpina1e expression by modulating these two essential epigenetic modification enzymes. We found that AKG supplementation did not affect RNA modification as indicated by unchanged mRNA expression of m6A-related enzymes in primary hepatocytes. Conversely, the level of H3K27me3 on serpina1e promoter and gluconeogenesis enzyme flux was decreased by AKG. Notably, these AKG-induced inhibitions were abolished by JMJD3 knockdown, suggesting that JMJD3-H3K27me3 mediates the AKG-serpina1e pathway.

Our data suggest a model that dietary AKG acts on hepatocytes to inhibit hepatic gluconeogenesis by stabilizing the transcription of serpina1e through histone demethylation. What is puzzling is that modification of histone methylation occurs typically in the nucleus and further affects metabolic progress (*54*). It is reasonably well established that extracellular AKG does not cross plasma membranes, and esterified forms of AKG were used in the field to overcome this problem (*27*, *55*, *56*). However, consistent with our observations, several other groups also showed similar epigenetic effects of AKG treatment. For example, dietary AKG has been shown to induce beige adipogenesis by enhancing DNA demethylation of the *Prdm16* gene in mice (*8*). Drinking supplementation of AKG ameliorates age-related osteoporosis by regulating histone methylations in mice (*57*). AKG extracellular supplementation promotes murine embryo development through metabolic and epigenetic modulations (*58*). Notably, all these studies used AKG instead of membrane-permeable dimethyl-α-ketoglutarate, suggesting a surface receptor/sensor-dependent mechanism. Consistently, we recapitulated the findings that exogenous AKG cannot enter the cell membrane. Levels of AKG in mitochondrial-free cytosol significantly increased after exogenous AKG incubation, indicating an enhanced mitochondrial-to-cytosol AKG transportation. In line with this observation, the expression of SLC25A11, also known as oxoglutarate carrier, on mitochondrial membrane increased after AKG treatment. Notably, knockdown of SLC25A11 reversed the exogenous AKG-induced AKG level elevated in mitochondrial-free cytosol. Besides, knockdown of SLC25A11 abolished AKG-induced hepatic gluconeogenesis suppression. These data support the notion that extracellular AKG enhances mitochondrial-to-cytosol transportation of intracellular AKG, which subsequently stabilizes the transcription of serpina1e through the JMJD3-H3K27me3 pathway. The stimulatory effects of exogenous AKG on mitochondrial-to-cytosol transportation of intracellular AKG may serve as a common mechanism for dietary AKG-induced epigenetic changes.

Another important finding of our studies is identifying a previously unidentified receptor/sensor mediating epigenetic regulatory effects of exogenous AKG. We found that a member of purinoreceptors, P2RX4, directly or indirectly binds with extracellular AKG in hepatocytes. We also provided evidence that P2RX4 is required for AKG-induced hepatic gluconeogenesis suppression. Combining with our observations on mitochondrial-to-cytosol AKG transportation, P2RX4 may serve as a mediating cell surface receptor/sensor for exogenous AKG to regulate intracellular AKG transport. However, additional studies are warranted to further support this concept.

In conclusion, we found that systemic supplementation of AKG prevents diabetic elevation of blood glucose by inhibiting hepatic gluconeogenesis in a serpina1e-H3K27me3–dependent mechanism. Physiologically, the study demonstrates a key role of AKG in the regulation of glucose metabolism. From the perspective of application, this study showed the therapeutic potential of AKG in T2DM.

MATERIALS AND METHODS

Animals

Mice were housed in a temperature/humidity-controlled environment (23° ± 3°C/70 ± 10%) on a 12-hour light/12-hour dark cycle (6 a.m. and 6 p.m.). C57BL/6 mice were purchased from the Animal Experiment Center of Guangdong Province (Guangzhou, Guangdong, China). Unless otherwise stated, the mice were maintained ad libitum on standard mouse chow (protein 18.0%, fat 4.5%, and carbohydrate 58%; Guangdong Medical Science Experiment Center, Guangzhou, Guangdong, China) and drinking water. All groups in one experiment contained an individual mouse with the same strain and sex. C57BL/6 mice were used for long-term or acute experiments to investigate the effects of AKG on blood glucose. The liver-specific serpina1e KO mice (Alb-Cre crossed with Cas9 mice, then injected with serpina1e-sgRNA HBAAV) were generated on a C57BL/6 background. They were used to investigate the effects of short-term AKG administration. Care of all animals and procedures in South China Agricultural University were consistent with "The Instructive Notions with Respect to Caring for Laboratory Animals" issued by the Ministry of Science and Technology of the People's Republic of China and were approved by the Animal Subjects Committee of South China Agricultural University.

Primary hepatocyte preparation

The primary hepatocyte fraction was obtained from male C57BL/6 mice as described previously (*59*, *60*). Mice were anesthetized by isoflurane and then cut vertically until the liver, portal vein, and inferior vena cava were sufficiently exposed. The flow rate was increased to 7 to 9 ml/min with Hanks' balanced salt solution (HBSS). The entire volume of HBSS was perfused through the liver. When the reservoir was just about to run out of HBSS, 70 ml of the digestion medium was poured. Type IV collagenase (100 U/ml; 17104019, Thermo Fisher Scientific) was used for digestion, and the flow rate was about 8 ml/min. Dulbecco's modified Eagle's medium (DMEM) with 25 mM glucose and 10% fetal bovine serum (FBS) was used for isolation and plating, and viability as determined by trypan blue staining was >90% for all preparations. Cells were plated on collagen-coated (8 μg/cm^2) plates. After the cells attached, they were washed

once with DMEM-low and culture medium (with 10% FBS) was added again for 3 to 4 hours. Plating was conducted for the first 4 to 5 hours. Cells were kept in a serum-free medium containing 5 to 25 mM glucose overnight, and all cells were used within 30 hours of plating.

Primary tissue culture of liver

Mouse liver tissue slice obtained from 12-week-old male C57BL/6 mice fed with chow diet was cultured in high-glucose DMEM (11965175, Thermo Fisher Scientific, Carlsbad, CA, USA) at 37°C in a humidified atmosphere that contained 5% CO_2. The high-glucose DMEM was supplemented with 10% FBS (16000044, Thermo Fisher Scientific), streptomycin sulfate (100 mg/liter) (11860038, Thermo Fisher Scientific), and penicillin sodium (100,000 U/liter). The liver was sliced to about 200 μm with a vibration slicer (VF-300 Microtome, USA) and then cultured for further treatment.

Association between plasma AKG level and blood glucose in Chinese adults

This observational study was conducted in Huadong Sanatorium (Wuxi, China) and Zhujiang Hospital (Guangzhou, China) between 2018 and 2019. Forty-two Chinese volunteers (36 males and 6 females) aged 26 to 85 were recruited from Huadong Sanatorium (Wuxi, China) and Zhujiang Hospital (Guangzhou, China). All volunteers were required to complete a self-assessment form 1 week before sample collection, including age, gender, and symptoms of other diseases. Volunteers with other diseases that affect blood glucose level and diabetes treatment history were excluded. Each volunteer's blood samples were collected and stored in EDTA tubes. Plasma samples were obtained by centrifugation (4°C, 4000*g* for 20 min) and used for spectrophotometry detection of glucose. The whole test procedure was reviewed and approved by the Human Subjects Ethics Committee of Huadong Sanatorium, and written consent was obtained from each volunteer. The plasma AKG levels were measured by liquid chromatography–tandem mass spectrometry (LC-MS/MS) analysis (UPLC 1290-6470A QQQ LC-MS instrument, Agilent Technologies). For the two-tailed Pearson's correlation coefficient analysis, negative or positive values indicate a negative or positive correlation between human plasma metabolites, or metabolites and HbA1c. The shade of color indicates the strength of the correlation (light yellow to dark red indicates that the negative correlation is gradually increasing, and light blue to dark blue indicates that the positive correlation is gradually increasing). The shape of a circle or an oval indicates the strength of the correlation (the closer to the circle or oval, the weaker or stronger to the correlation).

RNA interference in primary hepatocyte

RNA interference was conducted as we previously described (*36*). The serpina1e siRNA and NC siRNA were purchased from GenePharma Co. Ltd. (Shanghai, China) and transfected into primary hepatocyte by using Lipofectamine reagents (Invitrogen, Carlsbad, CA, USA) according to the manufacturer's instructions. The sequences of siRNA targeting serpina1e are 5′-UGGCUCAUGCCUGAUGCUATT-3′ (sense) and 5′-UAGCAUCAGGCAUGAGCCATT-3′ (antisense). The sequences of siRNA targeting selenbp2 are 5′-CCGACGAGCAAAUCUCAUUTT-3′ (sense) and 5′-AAUGAGAUUUGCUCGUCGGTT-3′ (antisense). The sequences of siRNA targeting cyp4a12b are 5′-GGGCUUAUUCUGAUGUCAUTT-3′ (sense) and 5′-AUGACAUCAGAAUAAGCCCTT-3′ (antisense). The sequences of siRNA targeting cyp2c70 are 5′-CCAAGGGCACAAGUGUAAUTT-3′ (sense) and 5′-AUUACACUUGUGCCCUUGGTT-3′ (antisense). The sequences of siRNA targeting SLC25A11 are 5′-GCCACUUCUGCGCCAGCAUTT-3′ (sense) and 5′-AUGCUGGCGCAGAAGUGGCTT-3′ (antisense). The sequences of siRNA targeting SLC13A2 are 5′-GCUGCUACUGGCUUGGCUATT-3′ (sense) and 5′- UAGCCAAGCCAGUAGCAGCTT-3′ (antisense). The sequences of siRNA targeting JMJD3 are 5′-CCCUAACAAACCCUAUUAUTT-3′ (sense) and 5′-AUAAUAGGGUUUGUUAGGGTT-3′ (antisense). The sequences of siRNA targeting P2RX4 are 5′-GCUCAUCCGCAGCCGUAAATT-3′ (sense) and 5′- UUUACGGCUGCGGAUGAGCTT-3′ (antisense). The sequences of siRNA targeting P2RY14 are 5′-GCACAAGGCGUCUAACUAUTT-3′ (sense) and 5′- AUAGUUAGACGCCUUGUGCTT-3′ (antisense). The sequences of siRNA targeting P2RY2 are 5′-GCUCUCUAUAUCUUCCUAUTT-3′ (sense) and 5′- AUAGGAAGAUAUAGAGAGCTT-3′ (antisense). The sequences of NC siRNA are 5′-UUCUCCGAACGUGUCACGUTT-3′ (sense) and 5′-ACGUGACACGUUCGGAGAATT-3′ (antisense). An aliquot of transfected cells was collected to determine serpina1e gene expression. Another aliquot of transfected cells was treated with 0 or 100 μM AKG for intracellular experiments. Primary hepatocyte was transfected with NC siRNA or siRNA targeting gene for 24 hours.

Liver-specific serpina1e KO mouse model

AAV virus vector carrying paired sgRNAs (AAV-sgRNAs-serpina1e) targeting serpina1e (sgRNA binding sites with 20.1-kb interval were located in exons 1 to 5 of the serpina1e gene) was generated and packed by Cyagen (Suzhou, China). The serpina1e sgRNA-A1: ACACAGAGGCCACTCTATTGA, sgRNA-A2: CAGCACAGAGGTCCCTCATAT. Alb-Cre mice were crossed with LSL-Cas9-EGFP mice to generate Alb-Cre/LSL-Cas9-EGFP (Alb-Cas9), a mouse model with Cas9 selectively overexpressed in Alb-positive liver cells. For 6-week-old mice, male Alb-Cas9 mice were intraperitoneally injected with AAV-sgRNAs-serpina1e [1×10^{12} genome copies (GCs)/ml] to generate a liver-specific sepina1e deletion mouse model (Alb-serpina1e$^{-/-}$). At 12 weeks of age, HFD-fed male Alb-serpina1e$^{-/-}$ and control mice (LSL-Cas9-EGFP mice injected with AAV-sgRNAs-serpina1e) were intraperitoneally injected with saline or AKG (10 mg/kg) for 6 hours. Blood glucose was measured at 0, 1, 2, 3, 4, 5, and 6 hours. After AKG injection for 6 hours, PTT and ITT were performed. At the end of the experiment, serum was collected and centrifuged at 20,000*g* and 4°C for 20 min. The insulin and liver gluconeogenesis enzymes were tested after the mice were euthanized.

Western blot analysis

Western blot analysis was performed as described previously (*61*). Total protein lysates (20 μg) were immunoblotted with rabbit anti–p-FAK [1:1000; #3283, Cell Signaling Technology (CST)], rabbit anti-FAK (1:1000; #13009, CST), rabbit anti-SLC25A11 antibody (1:1000; ab80464, Abcam), rabbit anti-PCK1 antibody (1:1000; #12940S, CST), rabbit anti-G6Pase antibody (1:1000; NBP2-82857, Novus), rabbit anti-FBP antibody (1:1000; #59172S, CST), rabbit anti–p-Akt antibody (1:1000; Ser^{473}, AP0140, ABclonal), rabbit anti-Akt antibody (1:1000; #9272S, CST), rabbit anti-PHD3 antibody (1:1000; A8001, ABclonal), rabbit anti-P2RX4 antibody (1:2000; 13534-1-AP, ProteinTech), rabbit anti-P2RY2 antibody (1:1000; bs-4180R, Bioss), rabbit anti-P2RY14 antibody (1:1000; DF8662, Affinity), rabbit anti–COX IV antibody (1:1000; A11631, ABclonal),

rabbit anti-selenbp2 antibody (1:1000; bs-4200R, Bioss), rabbit anti-kdm6b antibody (1:2000; A12763, ABclonal), rabbit anti-Cyp2c70 antibody (1:1000; ARP94482-P050, Aviva), rabbit anti-SLC25A11 antibody (1:1000; ab80464, Abcam), rabbit anti-SLC13A2 antibody (1:1000; ab272568, Abcam), rabbit anti–β-tubulin (1:50,000; AP0064, Bioworld Technology Inc., St. Louis Park, MN, USA), followed by donkey anti-goat horseradish peroxidase (HRP)–conjugated secondary antibody or goat anti-rabbit HRP-conjugated secondary antibody (1:50,000; bs-0294D or bs-0295G, Bioss, Woburn, MA, USA). The levels of tubulin served as the loading control.

Relative quantitative PCR analysis

Real-time polymerase chain reaction (RT-PCR) assay was conducted as described previously (*61*). Total mRNA was extracted with the HiPure RNA Kit (R4130-02, Magen, China) and digested with deoxyribonuclease (DNase) I. The total mRNA (1 μg) was reverse-transcribed to complementary DNA (cDNA) by oligo(dT)18 primer. Then, SYBR Green relative quantitative RT-PCR (qRT-PCR) was performed according to published protocols (*62*). Results were normalized by the expression of housekeeping gene β-actin.

Absolute quantitative PCR analysis

Absolute qRT-PCR assay was performed according to previous papers (*36*, *63*). The cDNA samples from mouse liver tissues were first generated as described in relative qRT-PCR analyses. The C_t value of each gene was obtained for further analysis. The specific PCR amplification product was purified by electrophoresis and gel extraction by using an agarose gel recovery kit (D2111-02, Magen BioSciences, Waltham, MA, USA) to generate a standard curve for serpina1e gene. The DNA concentration of each product was measured by NanoDrop (2000c, Thermo Fisher Scientific). The absolute copy number of each sample was calculated according to the following formula: $C = A/B \times 6.02 \times 10^{14}$, where A is the concentration obtained by OD260 (optical density at 260 nm) analysis (ng/μl), B is the molecular weight of the synthesized DNA (daltons), and C is the copy number of the synthesized DNA (copies/μl). Subsequently, 10-fold serial dilution was carried out on each purified PCR product seven times. The dilutions of each product were used as the templates for SYBR Green qRT-PCR to target the gene by using an ample amount of the abovementioned primers. The standard curve of each gene was plotted as a linear regression of the C_t values versus the log of the copy number. Eight-week-old male C57BL/6 mice were divided into two groups and then fed a chow diet or HFD for 12 weeks. Eight-week-old DB mice were fed a chow diet for 12 weeks, and then serpina1e expression in the liver was tested by absolute quantitative PCR (qPCR).

ChIP and real-time PCR

Chromatin immunoprecipitation (ChIP) assays were performed with a ChIP kit (LOT3432949, Millipore) and performed according to certain protocols (*20*, *64*, *65*). Briefly, primary hepatocyte was fixed with 1% formaldehyde for 15 min and then lysed with lysis buffer. To shear the DNA, cell lysates were sonicated and the extracts were clarified by centrifugation method. After preclearing with protein G agarose beads, antibodies were added and incubated at 4°C overnight on a 360° rotator. Then, protein G agarose beads were added and rotated for 1 hour at 4°C to collect immunoprecipitated complexes. The samples were washed once with low-salt buffer, once with high-salt buffer, once with LiCl buffer, and then twice with tris-EDTA buffer, and they were finally eluted with elution buffer. After reversing cross-links between protein and DNA by heating at 65°C for 4 hours, the DNA was purified and subjected to RT-PCR analysis. DNA (total chromatin) was input as the endogenous control. The primers that were used to amplify the serpina1e promoter are 5′- GGGTGTTCTAACT-GCTTTCT-3′ (forward) and 5′-GTATTTAAGCAGTGGGAGCCA-3′ (reverse). The soluble chromatin supernatant was immunoprecipitated with anti-H3K27me3 (07-449, Millipore). Immunoprecipitated DNA and input DNA were analyzed by using qRT-PCR, and the results are presented as the percentage of input.

Mitochondrial DNA and metabolism gene

Total cellular DNA was extracted from mice liver with DNAzol reagent (Invitrogen, CA, USA) according to the manufacturer's instructions. Mitochondrial DNA copy number was determined by quantification of mitochondrial marker genes, including mitochondrially encoded ATP synthase membrane subunit 6 (ATPase6), cytochrome c oxidase subunit 2 (COX2), and mitochondrial encoded cytochrome b (mt-Cytb). The expression level of *ATPase6*, *COX2*, and *mt-Cytb* was tested by qRT-PCR and normalized to an intron of the nuclear-encoded β-globin gene. Mitochondrial metabolism was determined by quantification of mitochondrial metabolism genes, including *Tfam*, *Cox6a1* (cytochrome c oxidase subunit 6A1), *Atp5b*, *Ndufa6* [NADH (reduced form of nicotinamide adenine dinucleotide):ubiquinone oxidoreductase subunit A6], *UQCRC1* (ubiquinol-cytochrome c reductase core protein 1), and *SDH*.

Transcriptomics

Transcriptomics was performed as described before (*36*). At 12 weeks of age, male C57BL/6 mice were switched to HFD and received tap water or water supplemented with 2% AKG for 11 weeks. Samples from HFD male C57BL/6 mice liver tissue were used for transcriptomic signature analysis. Untargeted transcriptomic profiling was conducted on the Illumina platform by Novogene Co. Ltd. (Beijing, China). The liver tissue sample preparation procedures can be referred to the previously published protocol with minor revisions (*66*). First, RNA was extracted with the HiPure RNA Kit (R4130-02, Magen, China) and digested with DNase I. RNA integrity was assessed with the RNA Nano 6000 Assay Kit of the Bioanalyzer 2100 System (Agilent Technologies, CA, USA). Total RNA (3 μg per sample) was used for RNA sample preparations. Next, RNA sequencing libraries were generated using NEBNext Ultra RNA Library Prep Kit for Illumina (NEB, USA) following the manufacturer's recommendations, and index codes were added to attribute sequences to each sample. Last, further analysis was conducted. Genes with $\log_2 FC \geq 1$ and $-\log_{10} P$ value ≥ 1.3 were considered significant.

UPLC-Orbitrap-MS/MS analysis for metabolites

The methods were performed as described previously (*36*). One hundred microliters of serum was transferred to a 1.5-ml EP (Eppendorf) microtube with 500 μl of methanol (MS grade) and then added to each sample to fully remove protein. Serum metabolite content was analyzed using LC-MS/MS analysis (UPLC 1290-6470A QQQ LC-MS instrument, Agilent Technologies). For in vivo acute experiments, 12-week-old male mice were injected with saline, AKG (10 mg/kg), 5-BDBD (P2RX4 antagonist, 1 mg/kg, S9498, Selleck), and AKG + 5-BDBD for 6 hours, and then cytosol (mitochondrial-free) and mitochondrial AKG levels were measured by LC-MS/MS. For in vitro experiments, primary hepatocyte (PA treatment) was cultured

with vehicle + NC, vehicle + si-SCL25A11, ^{13}C-AKG (100 μM) + NC, or ^{13}C-AKG + si-SLC25A11 for 6 hours. The mitochondria are isolated from the cytoplasm, and the content of AKG in the cytoplasm and mitochondria is measured by LC-MS/MS.

AKG effects on STZ-induced T1D

Eleven-week-old male C57BL6/J mice were intraperitoneally injected with STZ (60 mg/kg) (S0130, Sigma-Aldrich, MO, USA) once a day for 7 days. One week later, the blood glucose levels were measured and the mice with blood glucose levels >450 mg/dl were considered diabetic; thus, they were chosen for the following studies. Mice were randomly divided into two groups according to body weight, age, and blood glucose. The selected mice received intraperitoneal injections of AKG (10 mg/kg) or saline. The blood glucose levels of the mice were recorded for 6 hours.

Effect of AKG on reducing blood glucose in DB mice

Twelve-week-old male DB mice were intraperitoneally injected with AKG (10 mg/kg) or saline. Blood glucose was measured at 0, 1, 2, 3, 4, 5, and 6 hours. At the end of the experiment, serum insulin level and liver PEPCK, G6Pase, and FBP protein expression and enzyme activity were examined.

GTT, PTT, and ITT

Intraperitoneal GTT and PTT were performed after overnight fasting. For GTT, an injection of glucose (1 g/kg body weight) was given to the mice, and blood glucose levels were measured subsequently at different time points. For PTT, an injection of pyruvate (1 g/kg body weight) was given to the mice, and blood glucose levels were measured subsequently at different time points. ITT was performed after 4 hours of fasting. The mice were intraperitoneally injected with a single dose of insulin (1 U/kg), after which the blood glucose levels were measured. At 12 weeks of age, mice were switched to HFD and received tap water or water supplemented with 2% AKG for 9 weeks, and then performed for GTT. After AKG was supplemented for 10 weeks, ITT was performed. After AKG was supplemented for 11 weeks, PTT was performed.

Serum insulin, HbA1c, NEFA, TG, and liver NEFA and TG enzyme activity assay

Serum levels of insulin were measured using enzyme-linked immunosorbent assay (ELISA) (CSB-E05071m, Cusabio Biotech Co. Ltd.), and HbA1c was measured using ELISA (MM-0159 M2, Jiangsu Meimian Industrial Co. Ltd.). The enzyme activity of PEPCK, FBP, and G6Pase was measured using commercially available kits according to the manufacturer's instructions (Solarbio, China). The serum and liver NEFA and TG content were measured using commercially available kits according to the manufacturer's instructions (Solarbio, China).

H&E staining and Oil Red O staining

Hematoxylin and eosin (H&E) staining was performed as described before (*61*). Briefly, an aliquot of gastrocnemius and gWAT was fixed with 10% formalin and embedded with paraffin. Then, fixed gastrocnemius and gWAT were sectioned and stained with H&E or Oil Red O (O0625, Sigma-Aldrich). Pictures of stained adipose tissue were obtained in the same location. Adipocyte sizes of 30 adipocytes were analyzed per section. Data from eight mice were averaged for each group.

mRNA stability analysis

mRNA stability analysis was performed as described previously (*67*). Briefly, 12-week-old mice were treated with actinomycin D (1 mg/kg) (Sigma-Aldrich, A9415) to inhibit mRNA transcription. After treatment, the liver was collected and RNA samples were extracted for reverse transcription. The PEPCK, G6Pase, and FBP mRNA transcript levels of interest were detected by qPCR.

HGP assays

HGP assays were performed as previously described in primary mouse hepatocytes (*68*). Briefly, primary hepatocytes were cultured in 12-well plates at 2×10^5 cells per well and cultured at 37°C and 5% CO_2 overnight in serum- and hormone-free medium (11150-059, Invitrogen). After serum/hormone starvation, hepatocytes were washed twice with warm phosphate-buffered saline (PBS) (37°C). $PBS^{+/+}$ was replaced with 1 ml of glucose production buffer [consisting of glucose-free DMEM (pH 7.4) without phenol red supplemented with 20 mM sodium lactate, 2 mM sodium pyruvate, 2 mM L-glutamine, and 15 mM Hepes]. Cells were incubated at 37°C for 6 hours with or without 0.1 mM 8pCPT–adenosine 3′,5′-monophosphate (cAMP)-(4-chlorophenylthio)adenosine 3′,5′-cyclic monophosphate sodium salt) and/or 100 mM insulin, 0.2 ml of medium was collected, and glucose concentration was measured with a colorimetric glucose assay kit. Glucose released into the medium was detected using an Amplex Red/Glucose Oxidase kit (Invitrogen) and quantified spectrophotometrically at 560 nm. Glucose levels in the medium were normalized to total cellular protein content in each well.

OXGR1 KO mouse model

We generated an OXGR1 global KO mouse model (OXGR1KO) by using the clustered regularly interspaced short palindromic repeats (CRISPR) method, as described before (*7*). Briefly, OXGR1KO mouse model was generated by Shanghai Model Organisms Center Inc. The guide RNAs targeting exon 4 of OXGR1 gene were designed using CRISPR-Cas9 strategy. The Cas9 mRNA was in vitro transcribed using the mMESSAGE mMACHINE T7 Ultra Kit (Ambion, TX, USA) according to the manufacturer's instructions. Two sgRNAs were designed to delete the OXGR1 protein-coding region using the online designer (http://crispr.mit.edu/). The target sequences of two sgRNAs were 5′-GTTTAACCTCTAACTTCCAC-3′ and 5′-TTAAAGGCTCGAAGGCTAAC-3′. The sgRNAs were in vitro transcribed using the MEGAshortscript Kit (Thermo Fisher Scientific, USA) and subsequently purified using the MEGAclear Kit (Ambion, Life Technologies). The mixture of Cas9 mRNA and sgRNAs was coinjected into zygotes of C57BL/6 mouse by microinjection. F0 mice were genotyped by PCR, using primer pairs: forward: 5′-TATACCAGCTGTTTTTCTTGTTGC-3′; reverse: 5′-GATGCGTGGCTGTTTATGTCA-3′. The genotype of positive F0 was confirmed by sequencing. The positive F0 mice were chosen and crossed with C57BL/6 mice to produce F1 mice.

Liver-specific serpina1e overexpression mouse model

The generation of serpina1e overexpression HBAAV8-serpina1e and control HBAAV8-GFP strains was conducted by Cyagen (Suzhou, China). Following DNA sequencing screening, the AAV plasmid was packaged into AAV serotype 8 virus by Cyagen (Suzhou, China). To specifically test whether liver serpina1e mediates the hepatic gluconeogenesis, serpina1e liver-specific overexpression mouse model ($serpina1e^{OE}$) was generated by selectively delivering

HBAAV8-serpina1e into the liver of WT mice. Briefly, 10 μl of HBAAV8-serpina1e (3.56×10^{12} GC/ml) or control HBAAV8-GFP (5.16×10^{12} GC/ml) was bilaterally injected into the exposed liver. After 2 weeks of surgery recovery, mice were switched to HFD and further divided into two groups, and the role of serpina1e in gluconeogenesis was determined.

Hyperinsulinemic-euglycemic mouse clamp

Clamp studies were performed by Yangling IDimple Biotechnology Co. Ltd. (request for technical support via enquiries, email IDimple@163.com). Briefly, a catheter was implanted in the jugular vein of mice under isoflurane anesthesia at 6 days before the experiments. After overnight (from 6 p.m. to 8 a.m.) fasting, conscious mice were infused with [U-^{13}C6]glucose (ZCI-CLM-1396, Shanghai Zzbio Co. Ltd.) at a rate of 3.13 μg/min for 120 min. Then, blood samples were collected from the tail vein for measurement of basal EGP. Afterward, clamping was conducted for 140 min with a 3-min primed infusion of insulin at 6.0 mU/kg per min and 11.9 μg/min [U-^{13}C6] glucose, followed by continuous infusion of insulin at 2.5 mU/kg per min and 4.96 μg/min [U-^{13}C6]glucose, as well as a variable infusion of 50% dextrose to maintain euglycemia (~120 mg/dl). Following the clamping procedure, the mice were anesthetized by sodium pentobarbital injection, and blood samples, liver, epididymal white adipose tissue (eWAT), and skeletal muscle (gastrocnemius and soleus) specimens were collected for future analysis.

Intracellular ^{13}C AKG tracing

[U-^{13}C]AKG (catalog number: CLM-2411-0, Cambridge Isotope Laboratories) was added to primary hepatocyte for the indicated times at a final concentration of 100 μM. Cells were washed and lysed directly in metabolite extraction buffer, snap-frozen in liquid nitrogen, and stored at −80°C until MS analysis was performed. Primary hepatocytes were cultured with 0.25 mM PA for 24 hours and then treated with vehicle or 100 μM ^{13}C-AKG for 10 min (~0.17 hours) and 0.5, 1, 2, 3, 6, 12, and 24 hours. Then, intracellular and medium ^{13}C-AKG level was measured.

SPR (Biacore systems) assay

Binding experiments was performed via an SPR (Biacore T200). Briefly, the series sensor chip SA (Sensor Streptavidin) (BR-1005-31, GE Healthcare Bio-Sciences, Sweden) was activated by injecting 1 ml of conditioned buffer (50 mM NaOH and 1 mol NaCl). Subsequently, AKG-PEG4 (3-[2-[2-[2-(2-Aminoethoxy)ethoxy]ethoxy] ethoxy]) was diluted in immobilization buffer [10 × HBS-EP+ (pH 7.4)] and immobilized on the chip at a flow rate of 10 μl/min for 3 min. The control groups were run using 200 μl of running buffer (10 × HBS-EP+ buffer [pH 7.4, consisting of 10 mM 4-(2-hydroxyethyl) piperazine-1-ethane-sulfonic acid (HEPES), 150 mM sodium chloride (NaCl), 3 mM Ethylene Diamine Tetraacetie Acid (EDTA), and 0.005% (v v−1) polysorbate 20 (P20)], deionized water, 1:9). Mice liver total protein sample (15 μg/ml) were recovered at a flow rate of 5 μl/min for 15 replicates. Then, all the fishing protein was collected to an EP tube and further analyzed by Western blot. The data were analyzed using Biacore T200 Evaluation Software (GE Healthcare Bio-Sciences, Sweden).

Mitochondrial membrane protein extraction and mitochondria isolation

For the mitochondrial membrane protein extraction, proteins were isolated according to the procedure of mitochondrial membrane protein extraction kit (BB-3158, BestBio). Mitochondria isolation from primary hepatocyte was according to the procedure of mitochondrial isolation kit (KGA827, Keygentec).

Statistics

Statistical analyses were performed using GraphPad Prism 7.0 statistics software (Chicago, IL, USA). Statistical analysis methods were chosen on the basis of the design of each experiment and indicated in the figure legends. The data were presented as means ± SEM. $P \leq 0.05$ was considered statistically significant.

SUPPLEMENTARY MATERIALS

Supplementary material for this article is available at https://science.org/doi/10.1126/sciadv.abn2879

View/request a protocol for this paper from *Bio-protocol*.

REFERENCES AND NOTES

1. P. Zimmet, Z. Shi, A. El-Osta, L. Ji, Epidemic T2DM, early development and epigenetics: Implications of the Chinese Famine. *Nat. Rev. Endocrinol.* **14**, 738–746 (2018).
2. L. He, H. Li, N. Huang, X. Zhou, J. Tian, T. Li, J. Wu, Y. Tian, Y. Yin, K. Yao, Alpha-ketoglutarate suppresses the NF-κB-mediated inflammatory pathway and enhances the PXR-regulated detoxification pathway. *Oncotarget* **8**, 102974–102988 (2017).
3. L. He, J. Wu, W. Tang, X. Zhou, Q. Lin, F. Luo, Y. Yin, T. Li, Prevention of oxidative stress by α-ketoglutarate via activation of CAR signaling and modulation of the expression of key antioxidant-associated targets in vivo and in vitro. *J. Agric. Food Chem.* **66**, 11273–11283 (2018).
4. J. L. Mangal, S. Inamdar, Y. Yang, S. Dutta, M. Wankhede, X. Shi, H. Gu, M. Green, K. Rege, M. Curtis, A. P. Acharya, Metabolite releasing polymers control dendritic cell function by modulating their energy metabolism. *J. Mater. Chem. B* **8**, 5195–5203 (2020).
5. T. D. Bhagat, D. Von Ahrens, M. Dawlaty, Y. Zou, J. Baddour, A. Achreja, H. Zhao, L. Yang, B. Patel, C. Kwak, G. S. Choudhary, S. Gordon-Mitchell, S. Aluri, S. Bhattacharyya, S. Sahu, P. Bhagat, Y. Yu, M. Bartenstein, O. Giricz, M. Suzuki, D. Sohal, S. Gupta, P. A. Guerrero, S. Batra, M. Goggins, U. Steidl, J. Greally, B. Agarwal, K. Pradhan, D. Banerjee, D. Nagrath, A. Maitra, A. Verma, Lactate-mediated epigenetic reprogramming regulates formation of human pancreatic cancer-associated fibroblasts. *eLife* **8**, e50663 (2019).
6. J. P. Morris IV, J. J. Yashinskie, R. Koche, R. Chandwani, S. Tian, C. C. Chen, T. Baslan, Z. S. Marinkovic, F. J. Sanchez-Rivera, S. D. Leach, C. Carmona-Fontaine, C. B. Thompson, L. W. S. Finley, S. W. Lowe, α-ketoglutarate links p53 to cell fate during tumour suppression. *Nature* **573**, 595–599 (2019).
7. Y. Yuan, P. Xu, Q. Jiang, X. Cai, T. Wang, W. Peng, J. Sun, C. Zhu, C. Zhang, D. Yue, Z. He, J. Yang, Y. Zeng, M. Du, F. Zhang, L. Ibrahimi, S. Schaul, Y. Jiang, J. Wang, J. Sun, Q. Wang, L. Liu, S. Wang, L. Wang, X. Zhu, P. Gao, Q. Xi, C. Yin, F. Li, G. Xu, Y. Zhang, G. Shu, Exercise-induced α-ketoglutaric acid stimulates muscle hypertrophy and fat loss through OXGR1-dependent adrenal activation. *EMBO J.* **40**, e108434 (2021).
8. Q. Tian, J. Zhao, Q. Yang, B. Wang, J. M. Deavila, M. J. Zhu, M. Du, Dietary alpha-ketoglutarate promotes beige adipogenesis and prevents obesity in middle-aged mice. *Aging Cell* **19**, e13059 (2020).
9. C. D. Tekwe, K. Yao, J. Lei, X. Li, A. Gupta, Y. Luan, C. J. Meininger, F. W. Bazer, G. Wu, Oral administration of α-ketoglutarate enhances nitric oxide synthesis by endothelial cells and whole-body insulin sensitivity in diet-induced obese rats. *Exp. Biol. Med. (Maywood)* **244**, 1081–1088 (2019).
10. B. P. Dick, A. Yousif, O. Raheem, W. J. G. Hellstrom, Does lowering hemoglobin a1c reduce penile prosthesis infection: A systematic review. *Sex Med. Rev.* **9**, 628–635 (2021).
11. W. S. Lai, R. M. Arvola, A. C. Goldstrohm, P. J. Blackshear, Inhibiting transcription in cultured metazoan cells with actinomycin D to monitor mRNA turnover. *Methods* **155**, 77–87 (2019).
12. R. Barnett, Type 1 diabetes. *Lancet* **391**, 195 (2018).
13. M. Hoang, J. W. Joseph, The role of α-ketoglutarate and the hypoxia sensing pathway in the regulation of pancreatic β-cell function. *Islets* **12**, 108–119 (2020).
14. D. Xiao, L. Zeng, K. Yao, X. Kong, G. Wu, Y. Yin, The glutamine-alpha-ketoglutarate (AKG) metabolism and its nutritional implications. *Amino Acids* **48**, 2067–2080 (2016).
15. X. Zhang, Y. Wang, H. Y. Ge, Y. J. Gu, F. F. Cao, C. X. Yang, G. Uzan, B. Peng, D. H. Zhang, Celastrol reverses palmitic acid (PA)-caused TLR4-MD2 activation-dependent insulin resistance via disrupting MD2-related cellular binding to PA. *J. Cell. Physiol.* **233**, 6814–6824 (2018).
16. M. Farshchian, A. Kivisaari, R. Ala-Aho, P. Riihilä, M. Kallajoki, R. Grénman, J. Peltonen, T. Pihlajaniemi, R. Heljasvaara, V. M. Kähäri, Serpin peptidase inhibitor clade A member 1

(SerpinA1) is a novel biomarker for progression of cutaneous squamous cell carcinoma. *Am. J. Pathol.* **179**, 1110–1119 (2011).
17. S. Tsujimoto, T. Ishida, T. Takeda, Y. Ishii, Y. Onomura, K. Tsukimori, S. Takechi, T. Yamaguchi, H. Uchi, S. O. Suzuki, M. Yamamoto, M. Himeno, M. Furue, H. Yamada, Selenium-binding protein 1: Its physiological function, dependence on aryl hydrocarbon receptors, and role in wasting syndrome by 2,3,7,8-tetrachlorodibenzo-p-dioxin. *Biochim. Biophys. Acta* **1830**, 3616–3624 (2013).
18. S. Straniero, A. Laskar, C. Savva, J. Härdfeldt, B. Angelin, M. Rudling, Of mice and men: Murine bile acids explain species differences in the regulation of bile acid and cholesterol metabolism. *J. Lipid Res.* **61**, 480–491 (2020).
19. D. N. Muller, C. Schmidt, E. Barbosa-Sicard, M. Wellner, V. Gross, H. Hercule, M. Markovic, H. Honeck, F. C. Luft, W. H. Schunck, Mouse Cyp4a isoforms: Enzymatic properties, gender- and strain-specific expression, and role in renal 20-hydroxyeicosatetraenoic acid formation. *Biochem. J.* **403**, 109–118 (2007).
20. P.-S. Liu, H. Wang, X. Li, T. Chao, T. Teav, S. Christen, G. Di Conza, W.-C. Cheng, C.-H. Chou, M. Vavakova, C. Muret, K. Debackere, M. Mazzone, H.-D. Huang, S.-M. Fendt, J. Ivanisevic, P.-C. Ho, α-Ketoglutarate orchestrates macrophage activation through metabolic and epigenetic reprogramming. *Nat. Immunol.* **18**, 985–994 (2017).
21. A. Cieslar-Pobuda, T. D. Ahrens, S. Caglayan, S. Behringer, L. Hannibal, J. Staerk, DNMT3B deficiency alters mitochondrial biogenesis and α-ketoglutarate levels in human embryonic stem cells. *Stem Cells* **38**, 1409–1422 (2020).
22. Z. Liang, R. L. Kidwell, H. Deng, Q. Xie, Epigenetic N6-methyladenosine modification of RNA and DNA regulates cancer. *Cancer Biol. Med.* **17**, 9–19 (2020).
23. S. Seok, Y. C. Kim, S. Byun, S. Choi, Z. Xiao, N. Iwamori, Y. Zhang, C. Wang, J. Ma, K. Ge, B. Kemper, J. K. Kemper, Fasting-induced JMJD3 histone demethylase epigenetically activates mitochondrial fatty acid β-oxidation. *J. Clin. Invest.* **128**, 3144–3159 (2018).
24. J. M. Martinez-Moreno, M. Fontecha-Barriuso, D. Martin-Sanchez, J. Guerrero-Mauvecin, E. Goma-Garces, B. Fernandez-Fernandez, S. Carriazo, M. D. Sanchez-Niño, A. M. Ramos, M. Ruiz-Ortega, A. Ortiz, A. B. Sanz, Epigenetic modifiers as potential therapeutic targets in diabetic kidney disease. *Int. J. Mol. Sci.* **21**, 4113 (2020).
25. X. Yin, S. Yang, M. Zhang, Y. Yue, The role and prospect of JMJD3 in stem cells and cancer. *Biomed. Pharmacother.* **118**, 109384 (2019).
26. E. E. Baracco, F. Castoldi, S. Durand, D. P. Enot, J. Tadic, K. Kainz, F. Madeo, A. Chery, V. Izzo, M. C. Maiuri, F. Pietrocola, G. Kroemer, α-Ketoglutarate inhibits autophagy. *Aging* **11**, 3418–3431 (2019).
27. Q. Yang, X. Liang, X. Sun, L. Zhang, X. Fu, C. J. Rogers, A. Berim, S. Zhang, S. Wang, B. Wang, M. Foretz, B. Viollet, D. R. Gang, B. D. Rodgers, M. J. Zhu, M. Du, AMPK/α-ketoglutarate axis dynamically mediates DNA demethylation in the Prdm16 promoter and brown adipogenesis. *Cell Metab.* **24**, 542–554 (2016).
28. F. R. Traube, D. Ozdemir, H. Sahin, C. Scheel, A. F. Gluck, A. S. Geserich, S. Oganesian, S. Kostidis, K. Iwan, R. Rahimoff, G. Giorgio, M. Muller, F. Spada, M. Biel, J. Cox, M. Giera, S. Michalakis, T. Carell, Redirected nuclear glutamate dehydrogenase supplies Tet3 with α-ketoglutarate in neurons. *Nat. Commun.* **12**, 4100 (2021).
29. E. B. Taylor, Functional properties of the mitochondrial carrier system. *Trends Cell Biol.* **27**, 633–644 (2017).
30. L. H. Lash, Mitochondrial glutathione transport: Physiological, pathological and toxicological implications. *Chem. Biol. Interact.* **163**, 54–67 (2006).
31. G. Osis, K. L. Webster, A. N. Harris, H. W. Lee, C. Chen, L. Fang, M. F. Romero, R. B. Khattri, M. E. Merritt, J. W. Verlander, I. D. Weiner, Regulation of renal NaDC1 expression and citrate excretion by NBCe1-A. *Am. J. Physiol. Renal Physiol.* **317**, F489–F501 (2019).
32. P. M. Deen, J. H. Robben, Succinate receptors in the kidney. *J. Am. Soc. Nephrol.* **22**, 1416–1422 (2011).
33. A. D. Qi, T. K. Harden, R. A. Nicholas, GPR80/99, proposed to be the P2Y(15) receptor activated by adenosine and AMP, is not a P2Y receptor. *Purinergic Signal.* **1**, 67–74 (2004).
34. C. Coddou, R. Sandoval, M. J. Hevia, S. S. Stojilkovic, Characterization of the antagonist actions of 5-BDBD at the rat P2X4 receptor. *Neurosci. Lett.* **690**, 219–224 (2019).
35. R. Berton, M. S. Conceição, C. A. Libardi, R. R. Canevarolo, A. F. Gáspari, M. P. Chacon-Mikahil, A. C. Zeri, C. R. Cavaglieri, Metabolic time-course response after resistance exercise: A metabolomics approach. *J. Sports Sci.* **35**, 1211–1218 (2017).
36. Y. Yuan, P. Xu, Q. Jiang, X. Cai, T. Wang, W. Peng, J. Sun, C. Zhu, C. Zhang, D. Yue, Z. He, J. Yang, Y. Zeng, M. Du, F. Zhang, L. Ibrahimi, S. Schaul, Y. Jiang, J. Wang, J. Sun, Q. Wang, L. Liu, S. Wang, L. Wang, X. Zhu, P. Gao, Q. Xi, C. Yin, F. Li, G. Xu, Y. Zhang, G. Shu, Exercise-induced α-ketoglutaric acid stimulates muscle hypertrophy and fat loss through OXGR1-dependent adrenal activation. *EMBO J.* **39**, e103304 (2020).
37. X. Cai, Y. Yuan, Z. Liao, K. Xing, C. Zhu, Y. Xu, L. Yu, L. Wang, S. Wang, X. Zhu, P. Gao, Y. Zhang, Q. Jiang, P. Xu, G. Shu, α-Ketoglutarate prevents skeletal muscle protein degradation and muscle atrophy through PHD3/ADRB2 pathway. *FASEB J.* **32**, 488–499 (2018).
38. M. Barrosse-Antle, C. Su, P. Chen, K. E. Boodhansingh, T. J. Smith, C. A. Stanley, D. D. De León, C. Li, A severe case of hyperinsulinism due to hemizygous activating mutation of glutamate dehydrogenase. *Pediatr. Diabetes* **18**, 911–916 (2017).
39. M. Willenborg, U. Panten, I. Rustenbeck, Triggering and amplification of insulin secretion by dimethyl alpha-ketoglutarate, a membrane permeable alpha-ketoglutarate analogue. *Eur. J. Pharmacol.* **607**, 41–46 (2009).
40. M. Thevis, A. Thomas, W. Schänzer, Insulin. *Handb. Exp. Pharmacol.* 209–226 (2010).
41. R. A. DeFronzo, Pathogenesis of type 2 diabetes mellitus. *Med. Clin. North Am.* **88**, 787–835 (2004).
42. N. Apostolova, F. Iannantuoni, A. Gruevska, J. Muntane, M. Rocha, V. M. Victor, Mechanisms of action of metformin in type 2 diabetes: Effects on mitochondria and leukocyte-endothelium interactions. *Redox Biol.* **34**, 101517 (2020).
43. D. Karásek, Pioglitazone. *Vnitr Lek* **66**, 121–125 (2020).
44. H. Schrem, J. Klempnauer, J. Borlak, Liver-enriched transcription factors in liver function and development. Part I: The hepatocyte nuclear factor network and liver-specific gene expression. *Pharmacol. Rev.* **54**, 129–158 (2002).
45. R. W. Carrell, D. A. Lomas, Alpha1-antitrypsin deficiency—A model for conformational diseases. *N. Engl. J. Med.* **346**, 45–53 (2002).
46. G. Huasong, D. Zongmei, H. Jianfeng, Q. Xiaojun, G. Jun, G. Sun, W. Donglin, Z. Jianhong, Serine protease inhibitor (SERPIN) B1 suppresses cell migration and invasion in glioma cells. *Brain Res.* **1600**, 59–69 (2015).
47. D. Huang, A. T. Cheung, J. T. Parsons, M. Bryer-Ash, Focal adhesion kinase (FAK) regulates insulin-stimulated glycogen synthesis in hepatocytes. *J. Biol. Chem.* **277**, 18151–18160 (2002).
48. T. Y. Liu, C. X. Shi, R. Gao, H. J. Sun, X. Q. Xiong, L. Ding, Q. Chen, Y. H. Li, J. J. Wang, Y. M. Kang, G. Q. Zhu, Irisin inhibits hepatic gluconeogenesis and increases glycogen synthesis via the PI3K/Akt pathway in type 2 diabetic mice and hepatocytes. *Clin. Sci.* **129**, 839–850 (2015).
49. B. Zdzisinska, A. Zurek, M. Kandefer-Szerszen, Alpha-ketoglutarate as a molecule with pleiotropic activity: Well-known and novel possibilities of therapeutic use. *Arch. Immunol. Ther. Exp.* **65**, 21–36 (2017).
50. S. J. Liu, H. L. Tang, Q. He, P. Lu, T. Fu, X. L. Xu, T. Su, M. M. Gao, S. Duan, Y. Luo, Y. S. Long, FTO is a transcriptional repressor to auto-regulate its own gene and potentially associated with homeostasis of body weight. *J. Mol. Cell Biol.* **11**, 118–132 (2019).
51. S. Ma, C. Chen, X. Ji, J. Liu, Q. Zhou, G. Wang, W. Yuan, Q. Kan, Z. Sun, The interplay between m6A RNA methylation and noncoding RNA in cancer. *J. Hematol. Oncol.* **12**, 121 (2019).
52. X. Zha, X. Xi, X. Fan, M. Ma, Y. Zhang, Y. Yang, Overexpression of METTL3 attenuates high-glucose induced RPE cell pyroptosis by regulating miR-25-3p/PTEN/Akt signaling cascade through DGCR8. *Aging* **12**, 8137–8150 (2020).
53. S. Majumder, K. Thieme, S. N. Batchu, T. A. Alghamdi, B. B. Bowskill, M. G. Kabir, Y. Liu, S. L. Advani, K. E. White, L. Geldenhuys, K. K. Tennankore, P. Poyah, F. S. Siddiqi, A. Advani, Shifts in podocyte histone H3K27me3 regulate mouse and human glomerular disease. *J. Clin. Invest.* **128**, 483–499 (2018).
54. A. Jambhekar, A. Dhall, Y. Shi, Roles and regulation of histone methylation in animal development. *Nat. Rev. Mol. Cell Biol.* **20**, 625–641 (2019).
55. G. Marino, F. Pietrocola, Y. Kong, T. Eisenberg, J. A. Hill, F. Madeo, G. Kroemer, Dimethyl α-ketoglutarate inhibits maladaptive autophagy in pressure overload-induced cardiomyopathy. *Autophagy* **10**, 930–932 (2014).
56. J. Zhao, L. Peng, R. Cui, X. Guo, M. Yan, Dimethyl α-ketoglutarate reduces CCl4-induced liver fibrosis through inhibition of autophagy in hepatic stellate cells. *Biochem. Biophys. Res. Commun.* **481**, 90–96 (2016).
57. Y. Wang, P. Deng, Y. Liu, Y. Wu, Y. Chen, Y. Guo, S. Zhang, X. Zheng, L. Zhou, W. Liu, Q. Li, W. Lin, X. Qi, G. Ou, C. Wang, Q. Yuan, Alpha-ketoglutarate ameliorates age-related osteoporosis via regulating histone methylations. *Nat. Commun.* **11**, 5596 (2020).
58. Z. Zhang, C. He, L. Zhang, T. Zhu, D. Lv, G. Li, Y. Song, J. Wang, H. Wu, P. Ji, G. Liu, Alpha-ketoglutarate affects murine embryo development through metabolic and epigenetic modulations. *Reproduction* **158**, 123–133 (2019).
59. D. Glick, W. Zhang, M. Beaton, G. Marsboom, M. Gruber, M. C. Simon, J. Hart, G. W. Dorn 2nd, M. J. Brady, K. F. Macleod, BNip3 regulates mitochondrial function and lipid metabolism in the liver. *Mol. Cell. Biol.* **32**, 2570–2584 (2012).
60. R. Zhande, W. Zhang, Y. Zheng, E. Pendleton, Y. Li, R. D. Polakiewicz, X. J. Sun, Dephosphorylation by default, a potential mechanism for regulation of insulin receptor substrate-1/2, Akt, and ERK1/2. *J. Biol. Chem.* **281**, 39071–39080 (2006).
61. C. Zhu, P. Xu, Y. He, Y. Yuan, T. Wang, X. Cai, L. Yu, L. Yang, J. Wu, L. Wang, X. Zhu, S. Wang, P. Gao, Q. Xi, Y. Zhang, Y. Xu, Q. Jiang, G. Shu, Heparin increases food intake through AgRP neurons. *Cell Rep.* **20**, 2455–2467 (2017).
62. A. L. Bookout, D. J. Mangelsdorf, Quantitative real-time PCR protocol for analysis of nuclear receptor signaling pathways. *Nucl. Recept. Signal.* **1**, e012 (2003).
63. V. Chini, A. Foka, G. Dimitracopoulos, I. Spiliopoulou, Absolute and relative real-time PCR in the quantification of tst gene expression among methicillin-resistant Staphylococcus aureus: Evaluation by two mathematical models. *Lett. Appl. Microbiol.* **45**, 479–484 (2007).

64. Q. Zhang, H. Long, J. Liao, M. Zhao, G. Liang, X. Wu, P. Zhang, S. Ding, S. Luo, Q. Lu, Inhibited expression of hematopoietic progenitor kinase 1 associated with loss of jumonji domain containing 3 promoter binding contributes to autoimmunity in systemic lupus erythematosus. *J. Autoimmun.* **37**, 180–189 (2011).
65. Y. Y. Lee, M. T. Mok, W. Kang, W. Yang, W. Tang, F. Wu, L. Xu, M. Yan, Z. Yu, S. D. Lee, J. H. M. Tong, Y. S. Cheung, P. B. S. Lai, D. Y. Yu, Q. Wang, G. L. H. Wong, A. M. Chan, K. Y. Yip; K. F. To, A. S. L. Cheng, Loss of tumor suppressor IGFBP4 drives epigenetic reprogramming in hepatic carcinogenesis. *Nucleic Acids Res.* **46**, 8832–8847 (2018).
66. D. Parkhomchuk, T. Borodina, V. Amstislavskiy, M. Banaru, L. Hallen, S. Krobitsch, H. Lehrach, A. Soldatov, Transcriptome analysis by strand-specific sequencing of complementary DNA. *Nucleic Acids Res.* **37**, e123 (2009).
67. X. Wang, R. Wu, Y. Liu, Y. Zhao, Z. Bi, Y. Yao, Q. Liu, H. Shi, F. Wang, Y. Wang, m(6)A mRNA methylation controls autophagy and adipogenesis by targeting Atg5 and Atg7. *Autophagy* **16**, 1221–1235 (2020).
68. E. P. Taddeo, S. R. Hargett, S. Lahiri, M. E. Nelson, J. A. Liao, C. Li, J. K. Slack-Davis, J. L. Tomsig, K. R. Lynch, Z. Yan, T. E. Harris, K. L. Hoehn, Lysophosphatidic acid counteracts glucagon-induced hepatocyte glucose production via STAT3. *Sci. Rep.* **7**, 127 (2017).

Acknowledgments
Funding: This work was supported by grants from the National Natural Science Foundation of China (31790411 to Q.J.), the Local Innovative and Research Teams Project of Guangdong Province (2019BT02N630 to G.S.), the China Postdoctoral Science Foundation (2021M701264 to Y.Y.), and the National Institute of Diabetes and Digestive and Kidney Diseases from NIH (R00DK107008 to P.X. and K01DK111771 to Y.J.). **Author contributions:** Y.Y., C.Z., and Y.W. were the main contributors in the conduct of the study, data collection and analysis, data interpretation, and manuscript writing. J.S., J.F., Z.M., P.L., W.P., C.Y., G.X., P.X., Y.J., and Q.J. contributed to the conduct of the study. G.S. contributed to the study design, data interpretation, and manuscript writing. **Competing interests:** The authors declare that they have no competing interests. **Data and materials availability:** All data needed to evaluate the conclusions in the paper are present in the paper and/or the Supplementary Materials.

Submitted 17 November 2021
Accepted 17 March 2022
Published 4 May 2022
10.1126/sciadv.abn2879